END

FILMED

DTIC

MICROCOPY RESOLUTION TEST CHART

NATIONAL BUREAU OF STANDARDS-1963-A

AFGL-TR-85-0099
ENVIRONMENTAL RESEARCH PAPERS, NO. 913

Determination of Ionospheric Electron Density Profiles From Satellite UV Emission Measurements, FY84

R. E. DANIELL   J. R. JASPERSE
D. J. STRICKLAND   H. C. CARLSON, Jr
D. T. DECKER

26 April 1985

DTIC
ELECTE
OCT 17 1985
S
B
D

DTIC FILE COPY

IONOSPHERIC PHYSICS DIVISION   PROJECT DMSP, 4643
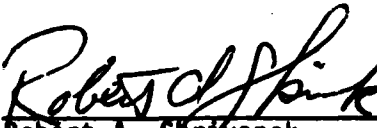AIR FORCE GEOPHYSICS LABORATORY
HANSCOM AFB, MA 01731

85 10 16 117

"This technical report has been reviewed and is approved for publication."

FOR THE COMMANDER

Herbert E. Whitney
Acting Branch Chief

Robert A. Skrivanek
Division Director

This document has been reviewed by the ESD Public Affairs Office (PA) and is releasable to the National Technical Information Service (NTIS).

Qualified requestors may obtain additional copies from the Defense Technical Information Center. All others should apply to the National Technical Information Service.

AD-A160 368

REPORT DOCUMENTATION PAGE

1a. REPORT SECURITY CLASSIFICATION		1b. RESTRICTIVE MARKINGS			
Unclassified					
2a. SECURITY CLASSIFICATION AUTHORITY		3. DISTRIBUTION/AVAILABILITY OF REPORT			
N/A		Approved for public release; distribution unlimited			
2b. DECLASSIFICATION/DOWNGRADING SCHEDULE					
N/A					
4. PERFORMING ORGANIZATION REPORT NUMBER(S)		5. MONITORING ORGANIZATION REPORT NUMBER(S)			
AFGL-TR-85-0099 ERP, No. 913					
6a. NAME OF PERFORMING ORGANIZATION	6b. OFFICE SYMBOL (If applicable)	7a. NAME OF MONITORING ORGANIZATION			
Air Force Geophysics Laboratory	LIS				
6c. ADDRESS (City, State and ZIP Code)		7b. ADDRESS (City, State and ZIP Code)			
Hanscom AFB Massachusetts 01731					
8a. NAME OF FUNDING/SPONSORING ORGANIZATION	8b. OFFICE SYMBOL (If applicable)	9. PROCUREMENT INSTRUMENT IDENTIFICATION NUMBER			
Space Division	SD				
8c. ADDRESS (City, State and ZIP Code)		10. SOURCE OF FUNDING NOS.			
P.O. Box 92960 Worldway Postal Center Los Angeles, CA 90009		PROGRAM ELEMENT NO.	PROJECT NO.	TASK NO.	WORK UNIT NO.
		35160F	DMSP	04	00
		62101F	4643	07	01

11. TITLE (Include Security Classification) Determination of Ionospheric Electron Density (Contd)

12. PERSONAL AUTHOR(S) *R. E. Daniell; *D. J. Strickland; *D. T. Decker; **J. R. Jasperse; and H. C. Carlson, Jr.

13a. TYPE OF REPORT	13b. TIME COVERED		14. DATE OF REPORT (Yr., Mo., Day)	15. PAGE COUNT
Scientific. Interim.	FROM Feb 84	TO Feb 85	1985 April 26	66

16. SUPPLEMENTARY NOTATION
*Computational Physics Inc., P.O. Box 360, Annandale, VA 22003
**Boston College, Chestnut Hill, MA 02167

17.	COSATI CODES		18. SUBJECT TERMS (Continue on reverse if necessary and identify by block number)
FIELD	GROUP	SUB. GR.	Global electron density, Ionosonde data
04	01		Satellite measurements, Total electron content
20	09		DMSP Ionospheric subregions (Contd)

19. ABSTRACT (Continue on reverse if necessary and identify by block number)

The possible use of satellite ultraviolet measurements to deduce the ionospheric electron density profile (EDP) on a global basis is discussed. A system concept is conceived and analyzed in which a UV sensor and automatic data processing software are developed for the Defense Meteorological Satellite Program (DMSP). The optical data and DMSP ion density and temperature data are utilized to deduce near real-time EDP in the neighborhood of the satellite orbital plane. The EDP data is used along with ground-based ionosonde data and Global Positioning Satellite total electron content data to specify the global EDP for systems users.

This report considers the following ionospheric subregions: (a) the daytime midlatitude ionosphere from 90 to 1000 km, (b) the nighttime midlatitude ionosphere from 200 to 1000 km, and (c) the auroral E layer from 90 to 200 km for undisturbed conditions. The spatial resolution considered for the daytime and nighttime EDP is at least one vertical profile for each square 500 km on a side and for the auroral E layer at least one vertical profile for each square 50 km on a side. Other ionospheric regions (Contd)

20. DISTRIBUTION/AVAILABILITY OF ABSTRACT	21. ABSTRACT SECURITY CLASSIFICATION	
UNCLASSIFIED/UNLIMITED ☐ SAME AS RPT. ☒ DTIC USERS ☐	Unclassified	
22a. NAME OF RESPONSIBLE INDIVIDUAL	22b. TELEPHONE NUMBER (Include Area Code)	22c. OFFICE SYMBOL
John R. Jasperse	(6170 861-3137	AFGL/LIS

DD FORM 1473, 83 APR EDITION OF 1 JAN 73 IS OBSOLETE.

11. (Contd)

Profiles From Satellite UV Emission Measurements. FY 84

---

18. (Contd)

Midlatitude ionosphere	Solar flux
Auroral E layer	Neutral wind
UV emissions	Optical emissions
Daytime airglow	Scale length
Background emissions	UV photometer
	UV spectrometer

---

19. (Contd)

were not considered because of frequent occurrence of irregularities and highly variable transport conditions.

During 1984 comparisons were continued between the hybrid daytime ionospheric model and experimental observations. These comparison studies indicate that: (1) the essential features of the EDP and certain UV emissions can be modelled, (2) the models are sufficiently sensitive to input parameters to yield poor agreement with observations when typical input values are used, (3) reasonable adjustments of the parameters can produce excellent agreement between theory and data for either EDP or airglow but not both; and (4) the qualitative understanding of the relationship between two input parameters (solar flux and neutral densities) and the model EDP and airglow features has been verified.

The development of a hybrid dynamic model for the nighttime midlatitude ionosphere has been initiated. This model is similar to the daytime hybrid model, but uses the sunset EDP as an initial value and calculates the EDP as a function of time through the night. In addition, a semi-empirical model has been developed, based on the assumption that the nighttime EDP is always well described by a modified Chapman function. This model has great simplicity and allows the EDP to be inferred in a straightforward manner from optical observations. Comparisons with data are difficult, however, because of the low intensity of the nightglow. Keywords, →

Contents

iii

Contents

Illustrations

iv

Tables

v

Determination of Ionospheric Electron Density Profiles From Satellite UV Emission Measurements. FY 84

1. EXECUTIVE OVERVIEW

1.1 The System Concept

In this report we discuss the possible use of satellite ultraviolet (UV) measurements to deduce the ionospheric electron density profile (EDP) on a global basis. The system concept is: (a) to develop and install a UV sensor on the *Defense Meteorological Satellite Program* (DMSP) satellite and to develop an associated automatic data *processing (software) system*, (b) to use the optical data together with DMSP ion density and temperature data to deduce the near real-time EDP in the neighborhood of the satellite orbital plane, and (c) to transmit this EDP data to be used together with ground-based ionosonde data and Global Positioning Satellite (GPS) total electron content (TEC) data to specify the global EDP for system users. The AWS 4D ionospheric model could be used to specify the global EDP. The additional ionosonde and TEC data would serve two purposes: to increase the EDP data base generated by the UV data, and to refine the UV based EDP where coincident data exist.

1.2 The Ionospheric Subregions

In this report we consider the following ionospheric subregions: (a) the day-time midlatitude ionosphere from 90 to about 1000 km, (b) the nighttime midlatitude ionosphere from about 200 to 1000 km, and (c) the auroral E layer from 90 to about 200 km for undisturbed conditions. The spatial resolution considered for the day-time and nighttime EDP is at least one vertical profile for each square 500 km on a side, and for the auroral E layer at least one vertical profile for each square 50 km on a side. The ionospheric subregions excluded from consideration either because of the high frequency occurrence of irregularities or highly variable trans-port conditions are the polar caps, the cusp, the auroral F region, and part of the equatorial nighttime region.

1.3 Summary of Work Accomplished in FY84

During 1984 we continued to make comparisons between our hybrid daytime ionospheric model and experimental observations. The purpose of these compari-sons has been to test our ability to model the EDP, to model the daytime airglow, and to produce agreement between theory and experiment for both the EDP and the airglow. In conjunction with these comparisons, we have begun to study how the model EDP and airglow intensities scale with changes in the input parameters. From the cases we have studied so far we have drawn the following conclusions:

(1) We can model the essential features of the EDP and certain UV emissions.

(2) The models are sufficiently sensitive to input parameters that using "typical" values produces poor agreement with observations.

(3) Reasonable adjustments of the input parameters can produce excellent agreement between theory and data for either EDP or airglow, but, in general, not both.

(4) We have verified our qualitative understanding of the relationship between two input parameters (solar flux and neutral densities) and the model EDP and airglow features.

We plan to make a systematic parameter study of our daytime model so that we can quantify the relationship between input parameters and the calculated EDP and optical emissions. We also expect to establish the sensitivity of the calculated airglow intensities to input parameters, and conversely, the accuracy of EDP's inferred from measured airglow intensities. We will continue to make compari-sons between our model calculations and EDP and airglow observations.

During 1984 we started the development of a hybrid dynamical model for the nighttime midlatitude ionosphere. This model is similar to the daytime hybrid model, but it uses the sunset EDP as an initial value and calculates the EDP as a

function of time through the night. This model is in the early stages of development, and no comparisons with data have been made. We have also been studying a semi-empirical model based on the assumption that the nighttime EDP is always well described by a modified Chapman function. One of the virtues of this model is its simplicity, which allows the EDP to be inferred from optical observations in a straightforward manner. However, we have made few comparisons with data, primarily because the nightglow is relatively weak, and observations with sufficient sensitivity and resolution have been rare. Consequently, we have concentrated on studying the detectability of the relevant nightglow features. Because these features are faint, background emissions and reflected light are a serious problem. We have determined the characteristics of the background and the capabilities that will be required of the observing instruments. We have concluded that the required capabilities do not appear to demand any extraordinary technology. During 1985 we will complete a thorough error analysis of the entire process of inferring the EDP from optical data. This will include observational uncertainties as well as model uncertainties. We will also study the use of in situ measurements to increase the reliability of the high altitude portion of the calculated EDP.

While concentrating on the midlatitude ionosphere, we largely neglected the auroral E layer during 1984. In previous years, we studied the nighttime auroral ionosphere, and this work was described by Strickland et al.[1] We have just begun to attack the daytime auroral problem, which combines the difficulties of the daytime midlatitude problem with those of the nighttime auroral problem. During 1985 we will merge our auroral model with our daytime model and begin to study the properties of the resulting combination.

2. BACKGROUND

2.1 Objective

The objective of this work is to determine the feasibility of deducing the EDP on a global basis in near real time from remote, passive optical and other measurements made from a satellite platform. It is also our objective to develop specific computer codes to convert the satellite measurements to electron density profiles. There are two types of computer codes that will be required to accomplish these objectives: research codes and operational codes. Research codes are codes which solve a set of equations for the EDP in a specific subregion of the ionosphere.

1. Strickland, D. J., Daniell, R. E., Jr., Decker, D. T., Jasperse, J. R., and Carlson, H. C., Jr. (1984) Determination of Ionospheric Electron Density Profiles From Satellite UV Emission Measurements, AFGL-TR-84-0140, AD A150734.

3

Generally, they require a large amount of computer time and storage on the AFGL CDC 7600. Operational computer codes are codes that require a much smaller amount of time and produce an approximate EDP for a specific set of ionospheric parameters. At AFGL we are developing research codes for each ionospheric subregion. According to the present plan, the operational computer codes will be developed elsewhere.

2.2 The System Concept

The development and use of an EDP sensor-software system requires the successful completion of a number of steps. They are:

(1) Performance of feasibility studies and the development of research-type computer codes for determining the EDP from remote passive optical and other measurements.

(2) Design, development and installation of a UV sensor on DMSP to scan several ionospheric emission features in the near nadir direction.

(3) Development and installation of operational computer codes to determine the EDP from DMSP data in near real time. The needed DMSP data are the several ionospheric emission features, the O^+ and H^+ ion densities, and the electron and ion temperatures. The optical emission features are to be measured by the SSUV sensor and the other data are to be measured by other DMSP sensors.

(4) Utilization of the DMSP EDP data with other data as an input to a large scale model to determine the global EDP in near-real time. For example, the AWS 4D ionospheric model could be used as the large scale model. Other useful data would be the ground-based ionosonde network providing bottomside EDP measurements and the GPS system providing TEC measurements. These additional data could provide an accurate calibration of the UV sensor whenever the DMSP passed near the region being sampled by these systems.

(5) Communication of the products of the global EDP model (bottomside profiles, topside profiles, TEC, f_oF_2, and so on) to system users. Systems in need of this information include HF communications systems, OTH systems, SPACETRACK radar systems, and classified systems.

The system concept is illustrated in Figure 1 where we show the DMSP and GPS satellites sensing the EDP with OTH and SPACETRACK radar systems utilizing the results.

4
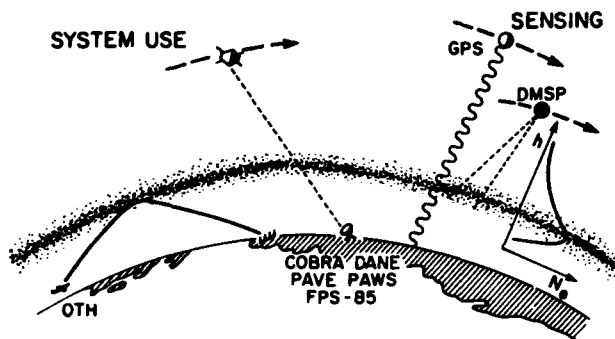
Figure 1. Global Electron Density Sensing
and System Use

2.3 Ionospheric Subregions

The ionosphere is generally divided into four altitude regions designated D,
E, F_1, and F_2 in order of increasing altitude. Three latitude regions—high, middle,
and low—are also recognized. At night the poleward boundary of the mid-latitude
region is defined by the midlatitude trough discovered by Muldrew[2] using Alouette I
topside sounder data. For our present purposes we identify the boundary between
the low and middle latitude regions as the latitude below which significant equatorial
EDP enhancements occur by day (Appleton Anomoly), and significant irregularities
characteristic of the equatorial region (such as equatorial spread F) are found at
night (generally within 20° of the geomagnetic equator; Fejer and Kelley[3]). Here
we take the 20° geomagnetic latitude contour as the nominal equatorward boundary
for the midlatitude ionosphere.

The system concept described in Section 2.2 is expected to be feasible in the
following four ionospheric subregions: (1) the daytime low latitude region from 90
to about 1000 km; (2) the daytime midlatitude region from 90 to 1000 km; (3) the
nighttime midlatitude region from about 200 to 1000 km; and (4) the auroral E-layer
from 90 to about 200 km for undisturbed conditions. (Note that sporadic E has been
excluded from consideration.) In Sections 3 through 5 we discuss the last three
subregions in some detail. The daytime low latitude region will be considered in
future years. The instrument characteristics imposed by the properties of these
three subregions are discussed in Section 6.

2. Muldrew, D. B. (1965) F-Layer Ionization troughs deduced from Alouette data,
      J. Geophys. Res. 70:2635.

3. Fejer, D.G., and Kelley, M.C. (1980) Ionospheric irregularities,
      Rev. Geophys. Space Phys. 18:401.

2.4 Early Work

Most of our early work was directed toward developing and assessing the feasibility of the system concept described above. This has involved the development of several computer codes for modeling the ionosphere in the various ionospheric subregions described above. It has also involved acquiring data for comparison with the models, and assessing the uncertainties that are likely to be introduced in the process of inferring ionospheric properties from optical data.

The system concept calls for specifying the midlatitude daytime EDP from 90 to 1000 km in near real time. This will require an empirical model or data base developed from the first principles models which we have been developing and testing. In order for an ionospheric model to specify the ionosphere uniquely, it must be given the following information:

    (1) the solar extreme ultraviolet (EUV) flux,

    (2) the densities of N_2, O_2, and O,

    (3) the neutral wind and electric field, and

    (4) temperatures (T_e, T_i, and T_n).

Note that the part of the solar EUV spectrum that does most of the ionizing is assumed to maintain its spectral shape independent of solar activity. This means that the solar EUV flux (item 1) can be characterized by a single parameter: its energy content. Our own investigations and those by Meier, Anderson and colleagues[4] at the Naval Research Laboratory have demonstrated that observations from the near UV (NUV) to the EUV can be used to determine items 1 and 2. In particular, the atomic oxygen line at 1356 A and one or more of the N_2 LBH bands appear most useful. The temperature of the neutral atmosphere can be obtained with sufficient accuracy from models. However, the electron and ion temperatures (which are only important for determining the high altitude EDP) must be obtained from in situ measurements. It may also be possible to determine the electric field from in situ measurements. Neutral winds have been measured from the ground using optical emissions. The choice of methods for obtaining and using this information is a subject for future research. A more complete description of the midlatitude daytime problem and our solution to it is given in Section 3.

The midlatitude nighttime ionosphere presents a different problem. In this region there are several optical emission features which are directly related to the EDP. The most important ones are the atomic oxygen lines at 1356 A and 6300 A. The 1356 A feature is rather weak but should be observable by currently available instruments. It is most sensitive to the peak electron density and is relatively

---

4. Anderson, D. E., Jr., Meier, R. R., Feldman, P. D., and Gentieu, E. P. (1980) The UV dayglow 3, OI emissions at 989, 1027, 1152, 1304, and 1356 A, <u>Geophys. Res.</u> Lett. 7:1057.

insensitive to the altitude of the peak. The 6300 A feature is sensitive to both the altitude and magnitude of the density peak. It is generally one or two orders of magnitude brighter than the 1356 A line. Unfortunately, the 6300 A line suffers from a rather large background made up of light reflected from clouds and the ground. The reflected light comes from astronomical sources (the moon, the stars, and the zodiacal light), OH airglow bands, and the 6300 A line itself. This means that the measurement of the 6300 A line involves monitoring the background and determining the albedo of the surface and clouds. Nevertheless, we feel that a properly designed photometer can make the measurement with sufficient accuracy for our purposes. We are considering two approaches to the problem of relating the observed intensities of these two features to the EDP. They are described in Section 4.

The auroral E layer (the EDP associated with the continuous or diffuse aurora) is similar in many respects to the daytime ionosphere. The main difference is that the ionization source is precipitating electrons rather than solar photons. The electrons deposit most of their energy between 90 and 200 km. As in the daytime ionosphere, we assume that the shape of the electron energy spectrum is known. However, there are two other parameters that must be determined from data: mean energy and total energy flux. As in the daytime, the most useful features are the OI 1356 A line and the N_2 LBH bands, which can provide the required information. The EDP also depends on the neutral composition. This must be determined by some other means (for example, a model). The current status of this problem is discussed in Section 5.

In addition to developing ionospheric models, we have searched for relevant experimental data to test our models and the overall system concept. Of particular interest are satellite experiments which carried either optical experiments or topside sounders. A chart of all such satellites known to us is shown in Table 1. It also includes satellites planned or projected for the next decade. For each satellite, the table contains orbital information, instrument complement and period of operation to the extent that they are known.

2.5 Scale Lengths for Horizontal Gradients in the Electron Density

There is a vast range of horizontal gradients in the EDP, in both the E and F regions. Large gradients pose a problem to optical monitoring of the EDP. The largest problem will arise from plasma instabilities for which optical techniques will be insufficient. Gradients under quiescent conditions, if large enough, will restrict observing times (a problem for nighttime measurements). Gradients can also adversely affect interpretation of OI 1304 A data in the nighttime and auroral ionospheres.

7

Table 1. Satellite-Borne Ionospheric Remote Sensing Experiments

Satellite name Launch date	Orbital Parameters: period (min)	perigee apogee (km)	inclin. (deg.)	Instrument Description	Operational dates:
Alouette I 28 September 1962	105.4	996 1027	80.5	swept frequency ionosonde	
Alouette II 29 November 1965	121.4	502 2982	79.8	swept frequency ionosonde	
OGO-4 28 July 1967	98.1	412	86	photometers: 1050-1350 A, 1230-1350 A, 1350-1550 A, 6300, 6225, 5893, 5577, 3914, 2630 A; UV spectrometer	
ISIS-I 30 January 1969	128.4	524 3523	88.4	swept frequency ionosonde	
ISIS-II 1 April 1971	113.7	1358 1429	88.15	swept frequency ionosonde; photometers: 3914 and 5577 A, 6300 A	
STP 72-1 2 October 1972	100	740 740	98.3	photometers: 170-400 A, 400-800 A, 800-1050 A, 1150-1400 A, 1220-1400 A	
AE-C (Explorer 51) 13 December 1973	132.4	155 4297	68.1	photometer: 7318, 6300, 5577, 5200, 4278, 3371 A	
AE-D (Explorer 54) 6 October 1975	118.5	141 3093	90	photometers: 5577 & 6300 A	
ISS-b 16 February 1978	107	972 1220	70	swept frequency ionosonde	
S3-4 16 March 1978	88.5	160 260	96.5	spectrometers: UV: 1620-2900 A, VUV: 1070-1930 A; photometer: 1216,1340,1550, 1750 A	

8

Table 1. Satellite-Borne Ionospheric Remote Sensing Experiments (Contd)

Satellite name Launch date	Orbital Parameters			Instrument Description	Operational dates
	period (min)	perigee apogee (km)	inclin. (deg.)		65 70 75 80 85 90 95 2000
STP 78-1 24 February 1979	96.5	600 600	97.7	spectrometer: EUV: 300-1400 A	++
Hilat 27 June 1983	102	850 850	82.2	imaging spectrometer: VUV: 1150-2000 A photometers: 3914, 6300 A	+ +
Space Shuttle (ISO on Spacelab 1) 28 November 1983	90?	300? 300?	?	imaging spectrometer: UV, visible, IR: 300-12,700 A	+
Projected Satellites					
Polar Bear	101?	830?	987	imaging spectrometer: VUV: 1150-2000 A imaging photometers: 3914, 6300 A	?──>
RAIDS	101?	830?	987	limb imaging spectrometers: EUV: 550-1100 A FUV: 1250-1550 A limb scanning spectrometers: MUV: 1900-3400 A NUV: 3000-4000 A NIR: 5577-8450 A limb scanning photometers: 5890, 7774, 6300 A	?──>
DMSP	101?	830?	987	imaging spectrometer: VUV: 1150-2000 A photometers: 3914,6300 A	?↑

We introduce OI 1304 A into the discussion since it is one of the most promi-
nent features in the UV and contains the same useful information found at 1356 A.
Since it is brighter than OI 1356 A, it is particularly attractive under nighttime and
weak auroral conditions. The radiation, however, experiences severe multiple
scattering which makes analysis difficult. In the absence of large EDP horizontal
gradients, the problem is one of simply modeling one-dimensional photon transport,
a challenging problem in itself (Strickland and Donahue,[5] Strickland and Rees,[6]
Meier and Lee[7]). Analysis of OI 1304 A data in regions of strong EDP gradients
may be complicated by horizontal photon transport effects. Quiescent EDP gradients
can be correlated with gradients in the production of 1304 A (as well as 1356 A)
photons. Such gradients, if strong enough, reduce emission from the higher produc-
tion regions and increase it elsewhere as photon transport sets up a net horizontal
flux out of the high production regions. Figure 2 illustrates the effect within an
auroral arc. The data were obtained by Huffman and colleagues[8] using a nadir
viewing FUV spectrometer onboard satellite S3-4. There is a clear broadening of
the 1304 A profile compared to the optically thin features.

Gradients to be addressed under quiescent conditions may be listed under the
following headings:

  (1) Appelton anomaly (at night),

  (2) midlatitude trough (at night),

  (3) dawn and dusk terminators,

  (4) post midnight collapse, and

  (5) continuous aurora.

We will give examples of scale lengths for categories 1-3 and 5. We define the
scale length by

$$L = n_e \left(\frac{dn_e}{dh} \right)^{-1} \tag{1}$$

where h is horizontal distance. The expression applies to a fixed altitude. The
physical meaning of L is that it is the e-folding distance of n_e at the point of
application.

5. Strickland, D. J., and Donahue, T. M. (1970) Excitation and radiation transport
      of 1304 A resonance radiation. I. The dayglow, Planet Space Sci. 18:661.

6. Strickland, D. J., and Rees, M. H. (1974) The OI 1304 A and 1356 A emission
      in aurorae, Planet. Space Sci. 22:465.

7. Meier, R. R., and Lee, J. -S. (1982) An analysis of the OI 1304 A dayglow using
      a Monte Carlo resonant scattering model with partial frequency redistribution,
      Planet. Space Sci. 30:439.

8. Huffman, R. E., Leblanc, F. J., Larrabee, J. C., and Paulsen, D. E. (1980)
      Satellite vacuum ultraviolet airglow observations, J. Geophys. Res. 85:2201.
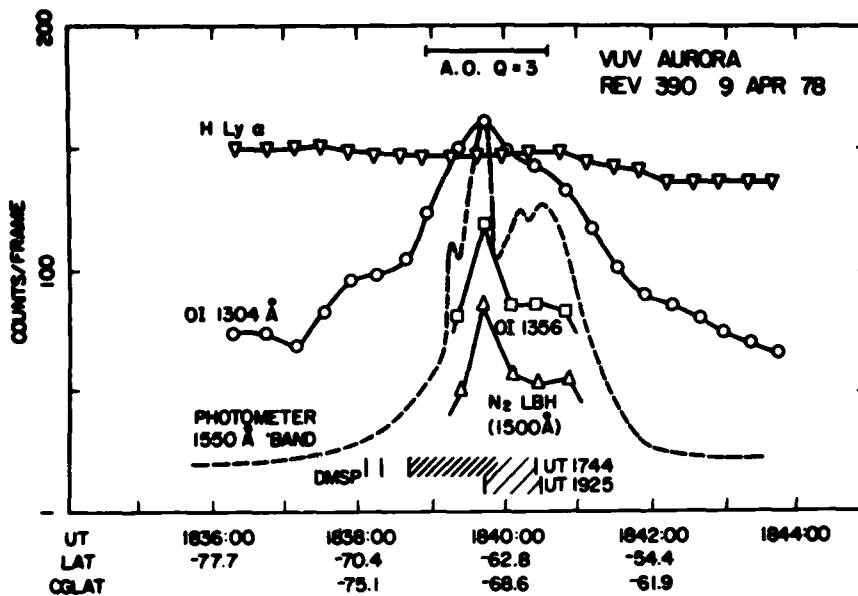
Figure 2. Auroral VUV Emissions as Observed by Photometer (1550 A) and Spectrometer (1100-2900 A) On-board the S3-4 Satellite (Huffman et al[8]). The location of the diffuse aurora (hatch marks) and auroral arcs (vertical lines) as determined from DMSP photographs are also shown. The optically thick feature (OI 1304 A) is clearly broadened in comparison to optically thin features such as OI 1356 A. This is due to the greater horizontal transport of optically thick photons

Item 4 may create a problem since it is a common occurrence, at least at low latitudes (Hanson and Carlson[9]). Figure 17 in last year's report (Strickland et al[1]) gives an example of the effect as a function of time. The example chosen shows a strong gradient in time over the lower F and upper E regions. This does not, however, translate simply into horizontal gradients. If the collapse (which was observed at one location - Arecibo) extended over large distances, large horizontal scale lengths would be present in spite of large time gradients. We have not suffi-ciently investigated this problem to estimate horizontal scale lengths.

Figure 3 shows an example of the horizontal variability in n_e^{max} for the Appelton anomaly in the nighttime F region. The results come from applying Eq. (1) to 911 A continuum data presented by Anderson et al.[10] These data appear in an inset in

9. Hanson, W. B., and Carlson, H. C. (1977) The ionosphere, from The Upper Atmosphere and Magnetosphere, National Academy of Sciences, Washington, D. C.

10. Anderson, D. E., Jr., Meier, R. R., and Weller, C. S. (1976) Observations of far and extreme ultraviolet OI emissions in the tropical ionosphere, Planet. Space Sci. 24:945.

11

Figure 3 (from Figure 1 in the Anderson paper). The horizontal axis is given in kilometers and refers to the data just to the right of the rightmost peak. A second inset in the figure shows the relationship between n_e^{max} and the 911 A intensity obtained from Eq. (1). We obtain a scale length of approximately 400 km at a distance of 300 km from the peak. The implications of such lengths will be discussed at the end of this subsection.
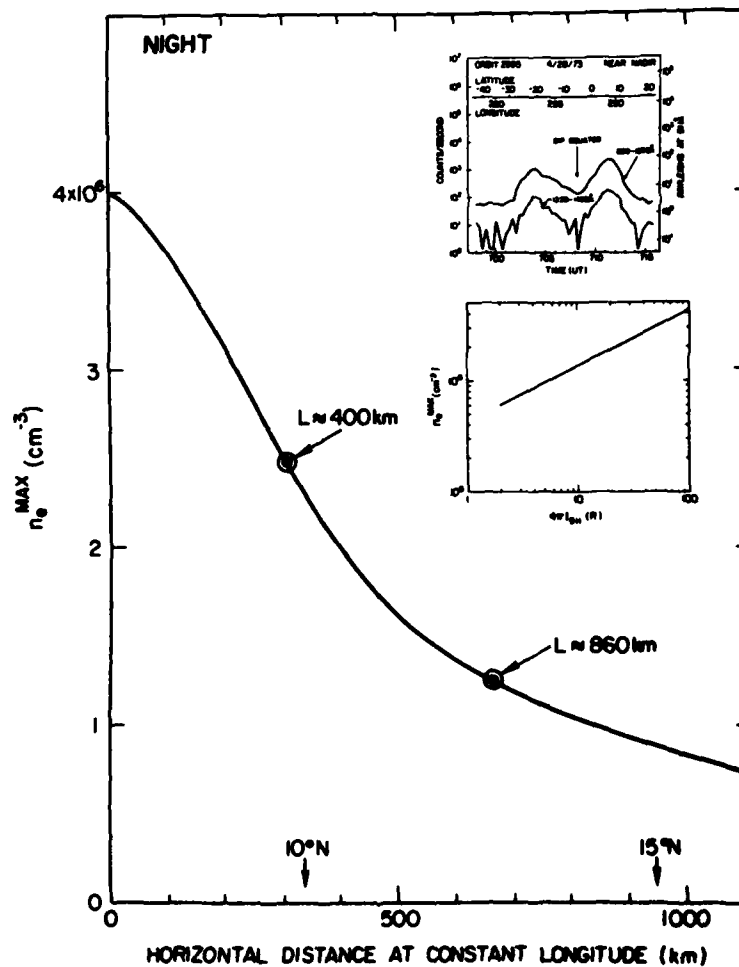

Figure 3. An Example of the Horizontal Variation of n_e^{max} in the Appleton Anomaly at Night. The insets show the original data (Anderson et al[10]) and the conversion from OI 911 A intensity to n_e^{max}. The horizontal scale length, L, is defined in the text

Figure 4 shows an example of how n_e varies through the midlatitude trough. The data were taken from Tulunay and Grebowsky[11] and were obtained with a plasma probe onboard the Ariel 3 satellite. The inset in Figure 4 is Figure 4 from their paper and shows several trough crossings. In the main body of Figure 4, curve 1 is replotted vs horizontal distance at an altitude of 550 km. Selected invariant magnetic latitudes are also shown along the x axis. Scale lengths of approximately 400 and 1400 km apply to the circled points on the plot. Two comments are worth making with regard to specific numbers such as these: first, they apply to one altitude and may not be the same at other altitudes near n_e^{max}, and second, we have shown only one example of the trough, which has scale lengths that may be quite different from those at other times. Notwithstanding these caveats, we expect that the chosen example does give a reasonable estimate of the kinds of lengths associated with the midlatitude trough.

Figure 5 illustrates the horizontal variation of n_e on the terminator. Sunrise has been chosen for producing the profile in the main part of the figure. The inset shows Figure 2 from Evans[12] and contains the data used to generate this profile. The chosen altitude is approximately 250 km. The contours in the inset are labeled by plasma frequency and had to be converted to density to generate the given profile. The smallest scale length along this curve is approximately 1200 km and is marked in the figure.

Shorter scale lengths occur along the terminator at E region heights due to the more rapid decay (in the case of sunset) of the EDP as the solar ionization source diminishes. This is illustrated in Figure 6 which gives the EDP at 140 km vs horizontal distance across the terminator. The profile was generated from bottom-side ionosonde data taken at Natal (6° S, 135° W) in August 1982. The data were provided by Jurgen Buchau of AFGL in the form of a figure containing numerous EDPs, each at a different local time. A scale length of ~715 km is obtained, nearly half of that at 250 km from the previous figure.

11. Tulunay, Y. K., and Grebowsky, J. M. (1978) The noon and midnight mid-latitude trough as seen by Ariel 4, J. Atmos. Terr. Phys. 40:845.

12. Evans, J. V. (1967) Midlatitude F-region densities and temperatures at sunspot minimum, Planet. Space Sci. 15:1387.
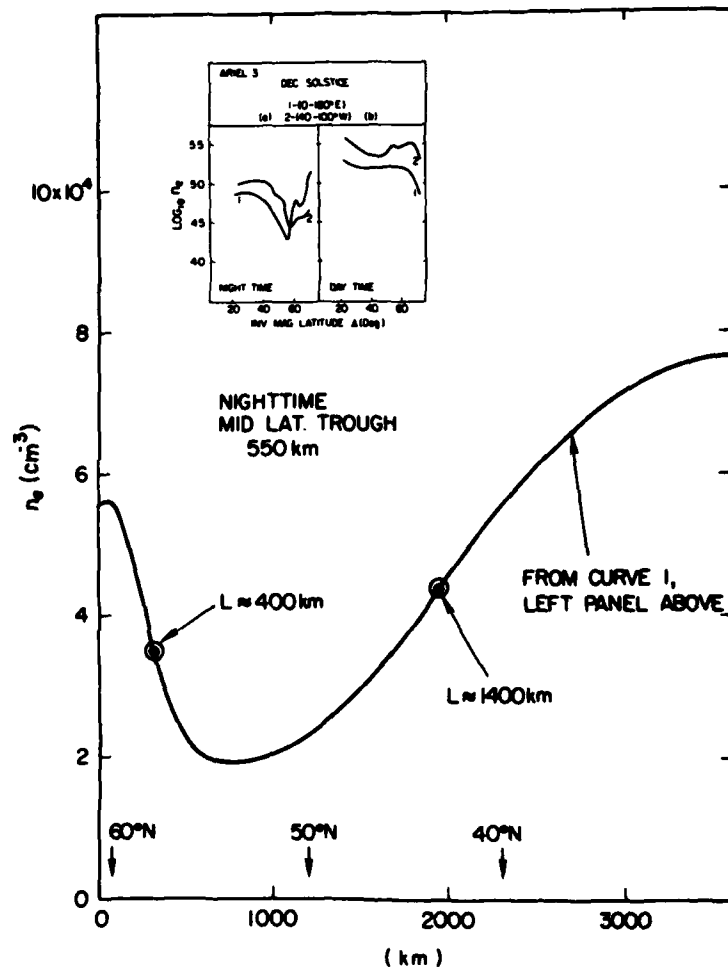
Figure 4. An Example of the Horizontal Variation of n_e in the Midlatitude Trough at Night. The inset shows the original data (Tulunay and Grebowsky[11]), which was obtained by a plasma probe on board the satellite Ariel 3. The horizontal scale length, L, is defined in the text
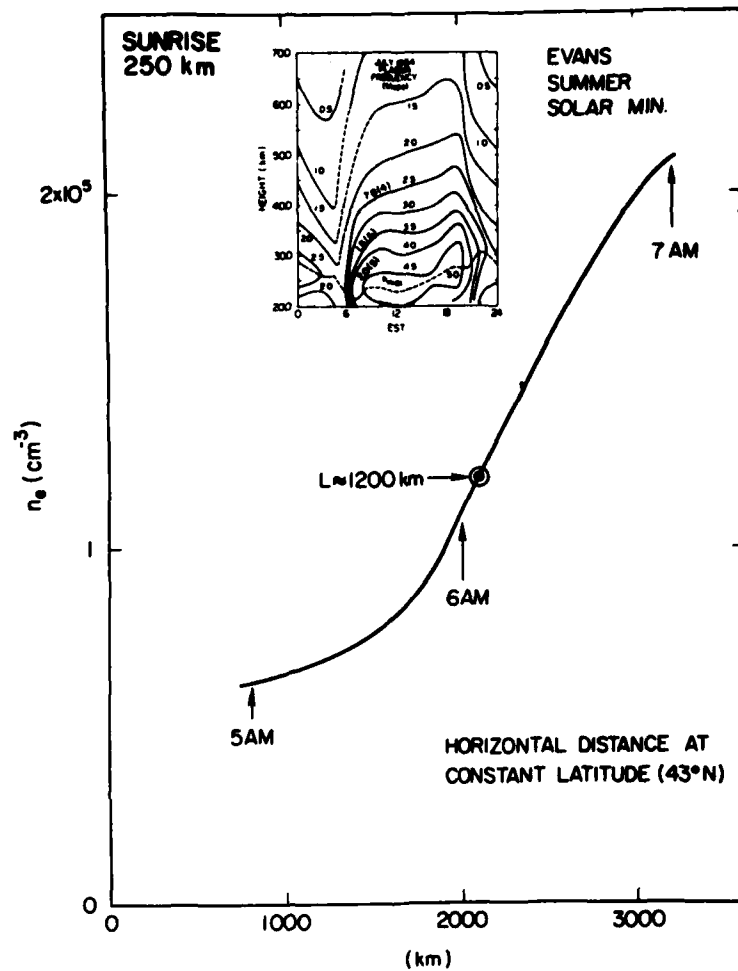
Figure 5. An Example of the Horizontal Variation of n_e at an Altitude of 250 km Through the Dawn Terminator. The inset shows the original data (Evans[12]), which was obtained by the incoherent scatter radar at Millstone Hill. The horizontal scale length, L, is defined in the text
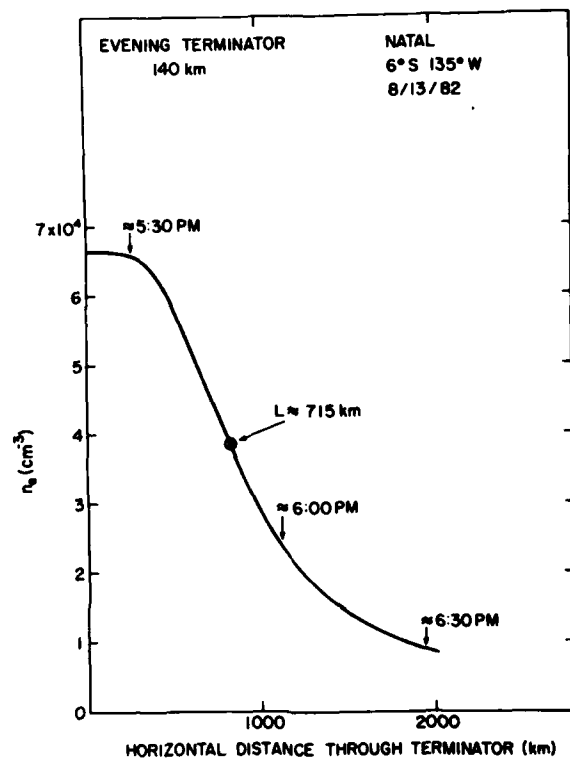
Figure 6. An Example of the Horizontal Variation of n_e at
an Altitude of 140 km Through the Evening Terminator.
See text for description of the original data

To estimate scale lengths for the continuous aurora, we make use of the work reported by Whalen[13] and Sharber.[14] In both papers, the authors find that Gaussian distributions can be applied to the latitudinal variation of the precipitated energy flux. Sharber shows that the mean energy of this flux is not constant over this profile using ISIS 2 electron spectrometer data. It has a value near 1 - 2 keV in the latitude region of maximum precipitation and decreases to either side. The data presented, however, do not exhibit as pronounced a Gaussian behavior in mean energy as in energy flux. Our point in introducing this mean energy variation is to note that it will have an effect on horizontal scale lengths in the EDP at a fixed altitude. Variation in energy flux alone will cause changes in overall magnitude of the EDP but will leave its peak unchanged in altitude. Variations in the mean energy will cause changes in the shape of the EDP including changes in peak altitude. Both changes together will increase horizontal scale lengths at some locations and decrease them at others. A location here is defined by some altitude and latitude within the Gaussian distribution.

The Gaussian expression for energy flux, as given by Whalen is

$$Q = Q_{max} \exp \left[-\frac{1}{2}\left(\frac{\Lambda - \Lambda_{max}}{\sigma}\right)^2 \right] \tag{2}$$

where Q is energy flux in, say, ergs/cm^2-sec, Λ is magnetic latitude and σ is the scaling parameter controlling width. Whalen obtained values from 0.7 to 2 from various sets of data. Sharber observed a value near 1 for the data he presented. We have examined the above distribution for two values of σ: 1.0 and 1.4. We have further converted latitude to horizontal distance at an altitude of 100 km to address the problem of scale lengths. For the discussion to follow, we assume a constant mean energy across the latitudinal distribution of the continuous aurora. In terms of lengths obtained directly from the two distributions, we obtain minimum values of ~ 130 and 170 km for the respective σ values of 1.0 and 1.4. These scale lengths apply to the variation in optical emission as viewed from a satellite since such emission is proportional to the energy flux. This applies to features such as OI 1356 A and the LBH bands.

13. Whalen, J.A. (1981) General characteristics of the auroral ionosphere, in *Physics of Space Plasmas*, Ed. by T.S. Chang, B. Coppi, and J.R. Jasperse, SPI Conference Proceedings and Reprint Series, 4, Scientific Publishers, Cambridge, Massachusetts

14. Sharber, J.R. (1981) The continuous (diffuse) aurora and auroral-E ionization in *Physics of Space Plasmas*, Ed. by T.S. Chang, B. Coppi, and J.R. Jasperse, SPI Conference Proceedings and Reprint Series, 4, Scientific Publishers, Cambridge, Massachusetts.

Scale lengths for the EDP may be obtained by taking the square root of the above profiles. The square root arises since to a good approximation, n_e varies as the square root of ion production in the E region. At a given altitude, this production has the same latitude dependence as the energy flux in the absence of changes in the mean energy. Resulting scale lengths are 170 km and 225 km for the above σ values.

Horizontal variations in n_e as illustrated in the paragraphs above should not impact required observing times except possibly in the trough where emission is very weak. This applies to all candidate optical features except OI 1304 A which is discussed in the next paragraph. With electron densities on the order of 10^4 cm^{-3} in the trough, several seconds of observing time will be required since such densities result in intensities at the sub-Rayleigh level. The DMSP satellite covers a distance of approximately 7.5 km in one second. For a scale length of 400 km, a signal should be recorded approximately every 200 km or every 27 sec. No greater rate is required for trough structure such as that shown in Figure 4. This rate will generally be sufficient to acquire the needed counts, although sufficiency depends on instrument sensitivity, geometry, and background. This was discussed in last year's AFSD report and is further discussed in Section 6 of this report. The shortest of the scale lengths presented above are for the continuous aurora. Unlike the trough, there is sufficient emission from this type of aurora to enable frequent measurements as DMSP is passing over its structure.

It is much more difficult to relate n_e scale lengths to 1304 A intensities affected by horizontal photon transport. We know that nighttime and auroral n_e scale lengths can be correlated to 1304 A production scale lengths. There is, however, no simple relationship between such lengths and the effect of horizontal transport due to the complicated process of multiple scattering within resonance lines. What is required to address the problem is a partial frequency redistribution 2D Monte Carlo model. The answer as to how much effect horizontal transport will have can be expected to depend on the altitude distribution of the source photons. Nevertheless, some rough estimates of the effect of horizontal photon transport can be made just from the data presented in this section. For photon production scale lengths on the order of 50 km or less, significant spreading of the nadir observed 1304 A intensity will occur. This statement is based on Figure 2 where such scale lengths exist within the auroral arc centered on 1839:40 UT. We observe a much less sharply peaked 1304 A maximum than at 1356 A or for the LBH bands. There does not seem to be much effect for scale lengths of 400 km or more based on a comparison of the 1304 A data with the optically thin 911 A continuum data shown in Figure 3. We are identifying the curve labeled 1220-1400 A as the 1304 A curve in spite of the fact that approximately 30 percent of the emission comes from OI 1356 A. The

18

variation of the 1304 A emission is not noticeably smaller than the variation of the 911 A continuum. Based on this observation, it appears that DMSP observed 1304 A intensities can be safely used (except for structured aurora) without taking into account horizontal transport. We should note that the only region of interest for recording the 1304 A intensity is the nighttime region.

3. DAYTIME MIDLATITUDE IONOSPHERE

3.1 Prior Work

For the daytime ionosphere no method is yet known for determining the ionospheric electron density profile (EDP) from 90 to 1000 km directly from nadir viewing of atmospheric optical emissions. Instead, an indirect method using optical emissions to adjust the parameters in such a model for the EDP will likely be necessary. We are studying such an indirect method for use in the daytime midlatitude ionosphere, an ionospheric subregion where previous modeling has shown great promise.

A prerequisite for developing such an indirect method is to study the relationship between optical emissions and the EDP. For that purpose, we began this study by developing research codes which calculate both the EDP and several daytime ultraviolet airglow emission features. We are using these codes to perform ab *initio calculations to qualify and quantify those parameters* which most directly and sensitively determine the EDP and the optical emissions. In FY83 we made a series of ab initio test calculations for the EDP and compared the results to two types of remote EDP measurements (Strickland et al[1]). In two cases the measurements were made by ground based ionosondes in coincidence with rocket measurements of the EUV solar flux, a crucial input for the EDP model. In both cases, we had good relative and absolute agreement between theory and the data. A third case, in which no input data was available, involved comparison with topside sounder measurements. While the relative agreement was good, the absolute agreement between theory and experiment was much poorer than in the other two cases.

Our tentative conclusions were that our EDP model accounted for the essential features of the EDP, but the quality of the absolute agreement with measured EDPs strongly depended on the availability of the input data necessary for the EDP model. In an indirect method, such as we are developing, it is this necessary input data that will be adjusted through the use of optical emission measurements.

By the end of FY83, we had our airglow code operating and initial tests had produced results consistent with measurements of UV daytime emission features.

19

3.2 The Modeling Approach

A general approach for calculating airglow and EDP would be to solve a system of kinetic equations for the electrons, ions and neutrals along with Poisson's equation for the electric field. Such a system of equations, suitable for treating the ionosphere, can be derived from the Liouville Equation (Jasperse[15]). However, solving such a system of equations even with present computers is not practical.

On the other hand, considering fluid equations only is not sufficient for studying the relationship between the EDP and optical emissions. While a fluid theory may suffice to provide such macroscopic variables as densities and drifts, the photoelectron flux, from which the daytime airglow is calculated, must be obtained from a kinetic theory. We have developed a first approximation to a hybrid theory in which a kinetic treatment for the electrons is coupled to a fluid treatment for the ions (Jasperse[15, 16, 17]).

The starting point for our hybrid theory is the non-linear kinetic equation:

$$\left\{ \frac{\partial}{\partial t} + \underset{\sim}{v} \cdot \nabla_r + \frac{1}{m_e} \underset{\sim}{X} \cdot \nabla_v \right\} f_e = S_e + \sum_{\beta} L_{e\beta}(f_e) + \sum_{\eta} J_{e\eta}(f_e) \qquad (3)$$

where $\underset{\sim}{X}$ is the force on an electron due to gravity and electric and magnetic fields, f_e is the one-particle distribution function for the electrons, $S_e \, d\underset{\sim}{r} \, d\underset{\sim}{v}$ is the rate at which electrons are produced at $(\underset{\sim}{r}, \underset{\sim}{v})$ due to effects external to the system $L_{e\beta}$ is the electron-neutral particle collision operator and $J_{e\eta}$ is the electron-charged particle collision operator. The sums on β and η are over the neutral and charged species, respectively. This kinetic equation is coupled with the following continuity equations for the various ion species:

$$\frac{\partial n_i}{\partial t} + \nabla \cdot (n_i \underset{\sim}{v_i}) = P_i(f_e) + L_i(f_e) \qquad (4)$$

where P_i is the ith ion production rate, L_i is the ith loss rate, n_i the ith ion density, and $\underset{\sim}{v_i}$ is the ion transport velocity.

15. Jasperse, J. R. (1976) Boltzmann-Fokker-Planck models for the electron distribution function in the earth's ionosphere, Planet. Space Sci. 24:33.

16. Jasperse, J. R. (1977) Electron distribution function and ion concentrations in the earth's lower ionosphere from Boltzmann-Fokker-Planck theory, Planet. Space Sci. 25:743.

17. Jasperse, J. R. (1981) The photoelectron distribution function in the terrestrial ionosphere in Physics of Space Plasmas, Ed. by T. S. Chang, B. Coppi, and J. R. Jasperse, SPI Conference Proceedings and Reprint Series, 4, Scientific Publishers, Cambridge, Massachusetts

In the daytime bottomside ionosphere ($z < 250$ km) transport can be ignored and in the steady-state approximation the continuity equation for an ion species simplifies to a balance between its production and loss rates. In our model we included the four most important ion species, O^+, N_2^+, O_2^+, and NO^+. The kinetic equation is simplified by expanding f_e, S_e, $L_{e\beta}$, and $J_{e\eta}$ in angles of the velocity vector and truncating to lowest order. After averaging over the angles of v the steady state result is:

$$O = S_{eo} + \sum_{\beta} L_{e\beta o}(f_e) + \sum_{\eta} J_{e\eta o}(f_e) \qquad (5)$$

a detailed balance in phase space between electron production and loss. For this study, we further simplified this non-linear bottomside kinetic equation by assuming a Maxwellian distribution for the thermal electrons and used the continuous slowing down (CSD) approximation to calculate the high energy photoelectron distribution function. It is from the calculated distribution function that the photoelectron flux can be derived.

The VUV daytime emissions that we are interested in—the LBH bands and the 1356 A feature—are produced essentially in the bottomside ionosphere. To calculate their intensities, we begin with the photoelectron flux, $F_o(e, z)$, calculated as a function of energy and altitude. The volume emission rate at altitude z is given by:

$$V_i(z) = n(z) \int F_o(E, z)\, \sigma(E)\, dE \qquad (6)$$

where n(z) is the density of the emitting species and $\sigma(E)$ is the corresponding cross section. For viewing situations and emission features where photon transport can be neglected, integration of $V_i(z)$ along the line of sight taking into account absorption gives us the column emission rate.

In the topside ionosphere ($z > 250$ km), the full time-dependent continuity equations (including transport) must be solved, although a simplification is achieved because only the dominant ion species, O^+, need be followed (Anderson[18]). By neglecting secondary production and radiative recombination the continuity equation is effectively decoupled from a kinetic equation for the electrons. Further, since the photoelectron flux in the topside is not used to calculate the optical emissions, we do not need to solve a kinetic equation but only the O^+ continuity equation.

---

18. Anderson, D. N. (1973) A theoretical study of the ionospheric F region equatorial anamoly, 1, Theory, Planet. Space Sci. 21:409.

In an intermediate region, around and below the F2 peak (200 - 300 km), we find that at lower altitudes the solution of the full O^+ continuity equation becomes a steady state solution locally produced. Further at higher altitudes in this region the four ion species calculated in the local steady-state approximation are dominated by O^+. When both our topside and bottomside codes use similar inputs their solutions can overlap and we produce a complete EDP (90 - 600 km) by a simple empirical merging of the two solutions.

While the simple approach outlined above is adequate for examining the relationship between the EDP and daytime airglow, we are investigating more involved procedures for calculating the EDP. For example, in our present approach, we produce EDPs to 1000 km by assuming a one species, O^+ topside ionosphere. It is known, however, that above 600 to 800 km H^+ becomes an important ionospheric constituent. We thus believe that treating both O^+ and H^+ will be necessary for producing an accurate EDP to 2000 km. Another improvement to our "zeroth order" calculation would be to remove the steady-state assumption used in the bottomside. The resulting solutions would allow bottomside modeling in the daytime near sunrise and sunset. Finally, a more sophisticated approximation would involve solving at all altitudes the multiconstituent ion continuity equations coupled with an electron kinetic equation. A suitable and useful electron kinetic equation might come from retaining the first two terms of the velocity angle expansions of F_e, S_e, $L_{e\beta}$, and $J_{e\eta}$ (Jasperse[17]).

3.3 Comparison Between Theory and Experiment

The key parameters of our models are: (1) the solar EUV flux; (2) the neutral atmosphere (N_2, O_2 and O densities); (3) the neutral wind and electric fields; and (4) the temperatures (T_e, T_i, and T_n). Items 1 and 2 dominate in the E region and lower F region while all four items are important at higher altitudes. These are the parameters referred to in Section 3.1 whose effects on the optical emissions and the EDP we wish to quantify. For the indirect method to produce accurate EDP, it is necessary to determine which of these parameters can be modeled, which can be adjusted by optical emission measurements, and which have to be adjusted by other measurements. We already know that since the airglow is a bottomside phenomenon other measurements will be necessary to help determine the topside EDP. In particular, on the DMSP satellite in situ electron density and temperature measurements will be absolutely crucial.

In FY84 we continued our comparisons between ab initio calculations and experimental observations. The purpose of these comparisons has been to test our ability to model the EDP, to model daytime airglow and to self-consistently produce agreement between theory and experiment for both the EDP and airglow. Of the five cases

22

we present here, the last three are also our initial efforts to see how the model
EDP and airglow scale with changes in the input parameters.

Our first case is a situation for which only EDP measurements from incoherent
scatter radar were available.

<u>Case One</u>: Millstone Hill, incoherent scatter radar, 8 April 1978. As in the case
of the comparison with topside sounder measurements all the input parameters for
our model were unknown and we had to attempt to estimate them. Using typical
values for these parameters we calculated the EDP. Figure 7 shows a comparison
with the EDP derived from an incoherent scatter measurement. In this case, the
predicted peak is around 50 km above the measured peak, and densities can be as
much as a factor of three in error. This is another example where input data
unavailability seemed to sharply reduce the absolute agreement between theory
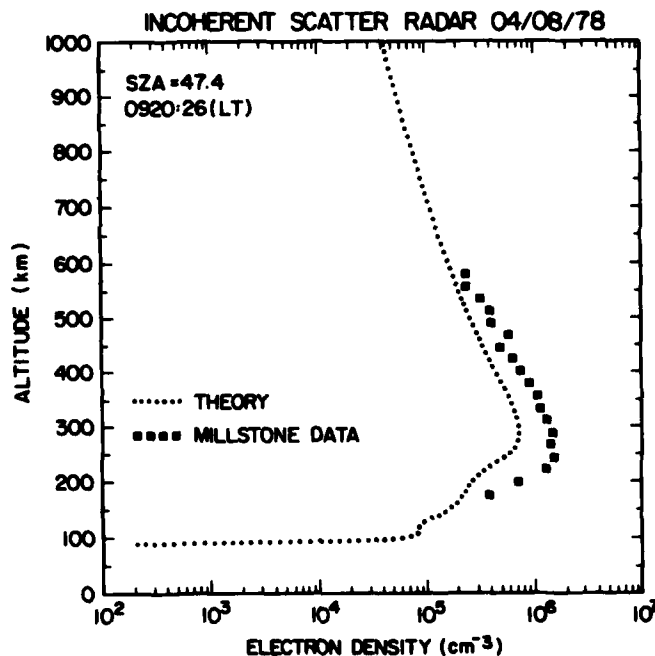and measurement.

Figure 7. Case One: Millstone Hill (incoherent
scatter radar), 8 April 1978. The poor agree-
ment between theory and observation is due to
the lack of input parameters for the model

23

Case Two: S3-4, Rev. 373, 8 April 1978. In this case we had detailed optical emission data from a nadir-looking VUV spectrometer flying on board DOD satellite S3-4 (Huffman et al[8]), but no simultaneous EDP or model parameter measurements. To calculate airglow emission intensities we needed, in addition to the parameters of our EDP model, the cross sections for the radiation processes. Because of the difficulty of laboratory measurements, some cross sections are still not well known. In particular, based on our own experience and Anderson et al[4] we used a cross section for the OI 1356 emission which is 0.6 times that measured by Stone and Zipf.[19] In Figure 8 we show airglow calculations from our ab initio model for features at nine wavelengths, along with S3-4 data for these same nine wavelengths.

S3-4 REV 373 DAYTIME 04/08/78

SZA = 29.06
1037 (LT)
■■■ AB INITIO THEORY
ERROR BARS ARE DATA
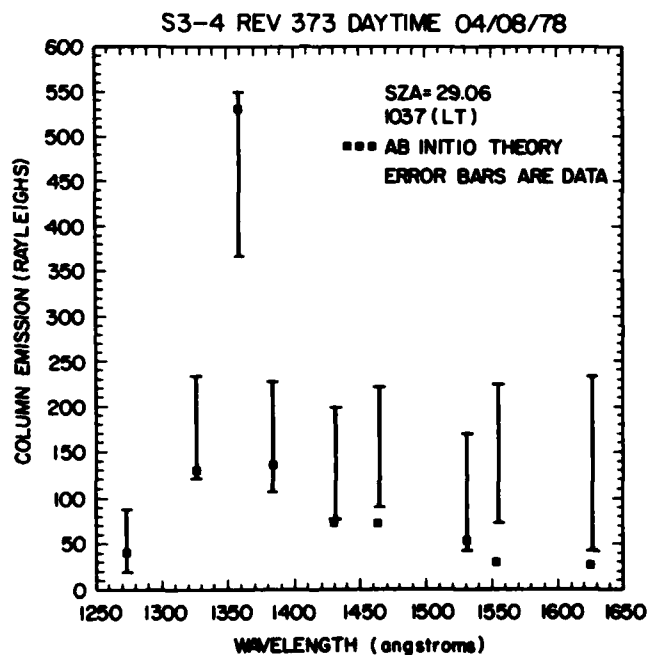
Figure 8. Case Two: S3-4, Rev 373, 8 April 1978. Calculated and observed column emission rates are compared at nine wavelengths. The large error bars on the S3-4 data are due to low count rates for this data. Reasonable agreement is obtained for features near 1356 A, but the agreement is worse at longer wavelengths where scattered light contaminates the data

19. Stone, E. J., and Zipf, E. C. (1974) Electron impact excitation on the $^3S^0$ and $^5S^0$ states of atomic oxygen, J. Chem. Phys. 60:4237.

We see that agreement is reasonable at short wavelengths, around the feature at 1356 A, but the agreement worsens at longer wavelengths where scattered light contamination makes data analysis more difficult. The large error bars on the data points are due to the statistical uncertainty resulting from the low count rates in the data. Moreover, the large error bars make it difficult to reach any conclusion about how "close" the theory is to measurement.

In Figure 9 we track the optical emissions at 1356 A as the satellite moves along its orbit in the noon-midnight plane, passing through midday in the northern hemisphere. We find that our completely ab initio calculation does a remarkable job in reproducing the observed emission produced over 60 degrees of geographic latitude. A similar plot for the feature at 1383 A (Figure 10) shows our theory running low over most of the latitude range.

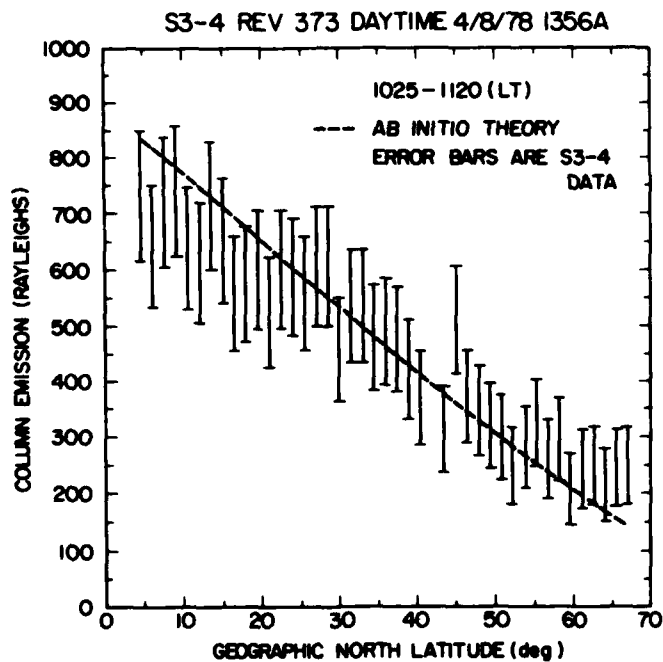For the remaining three cases both airglow and EDP measurements were available.

Figure 9. Case Two: A Comparison of Calculated and Observed OI 1356 A Emission Rates Along the S3-4 Orbital Track

S3-4 REV 373 DAYTIME 4/8/78 1383A
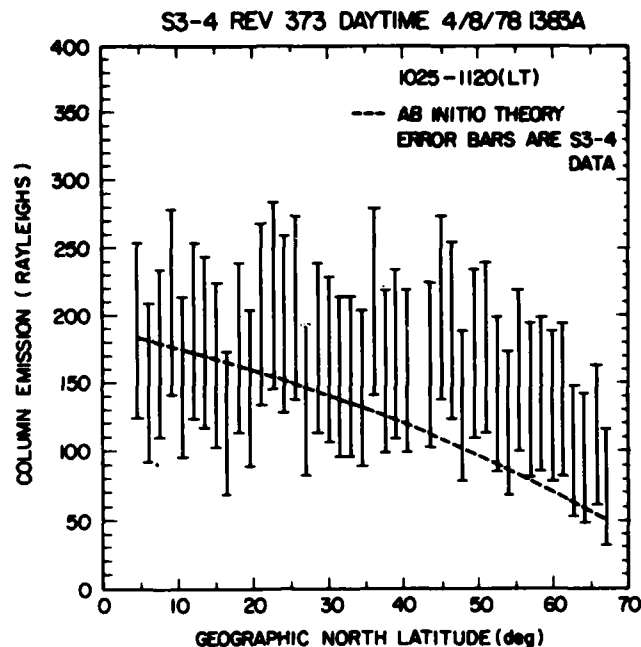
Figure 10. Case Two: A Comparison of Calculated
and Observed N_2 LBH 1383 A Emission Rates Along
the S3-4 Orbital Track

Case Three: HILAT Satellite, July 1983. In this case we attempt to model the
1356 A airglow observed from the HILAT satellite. On the date of observations the
satellite passed overhead near a ground based ionosonde at Millstone Hill making
near-coincident measurements of the EDP available.

The optical-emission measurements were made by the AIM sensor onboard
HILAT at 22:15:10 UT in Rev. 219. At this time, while crossing the latitude of
Millstone Hill, the satellite passed 16.4 degrees east of Millstone Hill. The Aim
sensor scans through 135 degrees along a path perpendicular to the satellite orbit,
in this case beginning its sweep looking east into darkness and ending looking west
into the bright limb (Figure 11). There is some uncertainty in the orientation of the
satellite, because in this orbit it was still oscillating on all three axes with the
amplitude of the oscillation unknown. If we assume that the sensor was pointed in
the nadir direction at the midpoint of the sweep, then the observed direction of the
bright limb is displaced by one data bin, 5.64 degrees, from its expected location.
We assume that this gives us an estimate of the satellite roll, and we assign error
bars of this magnitude to the directions of the calculated optical emissions. The
look direction from the satellite to Millstone Hill is 53.62 degrees W, placing

26

Millstone Hill in the foot of the bright limb. An uncertainty of 5.6 degrees in the look direction towards Millstone forces an uncertainty in the 1356 A flux of the order of 25 percent.
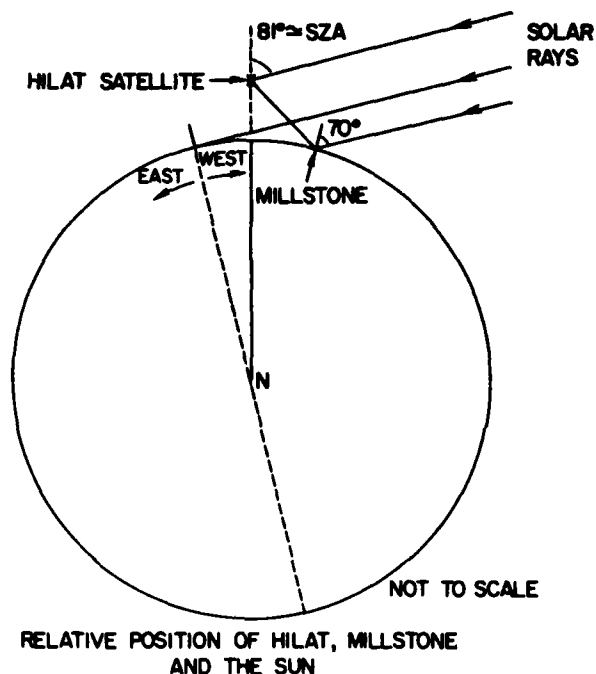
Figure 11. Case Three: HILAT Satellite and
Millstone Hill Ionosonde, July 1983

Our modeling began with a nadir calculation at the satellite location with a solar zenith angle (SZA) of 81 degrees. At this high SZA, the plane parallel approximation for the solar flux transport breaks down, resulting in an underestimation of the airglow emission rates. To get an upper bound for the airglow, a second nadir calculation was performed using an artificial value of the SZA, namely, the angle whose secant approximates the Chapman function at 81 degrees. At pixel 160 (different pixels are different look directions) we find that the two calculated intensities are, respectively, 1.2 and 1.5 times the observed 1356 A airglow intensity in that direction.

To calculate the column emission rate at some angle to nadir a plane parallel approximation for the atmosphere was used. Calculations at 10, 20, 30, 40 and 53.62 degrees (the look direction to Millstone Hill) are presented in Figure 12.

27

We see that the calculated emission profile reflects the profile of the data. At 53.62 degrees, however, the change in SZA along the look direction was large enough to call the plane-parallel approximation again into question. At that point we performed two airglow calculations to give bounds to the emission. One was based on the volume emission rate below the satellite, which with its higher SZA gives a lower bound to the airglow. The other calculation, based on the volume emission rate above Millstone, gives an upper bound. Figure 12 shows that the two results differ by a factor of two.
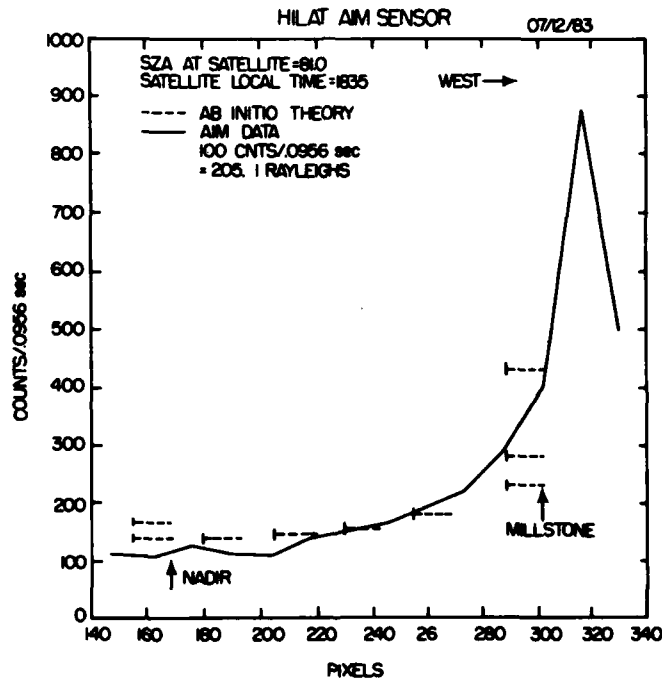
Figure 12. Case Three: A Comparison of Calculated and Observed OI 1356 A Emission Rates as a Function of the Nadir Angle of the Instrument Look Direction

We were interested in this particular sweep because a ground-based ionosonde had measured the EDP just a half hour before the satellite fly-over. While not an ideal coincidence either spatially or temporally, this did give us an opportunity to compare our ab initio calculations for the EDP and the airglow with observations of both quantities.

28

Comparison of the measured EDP with the ab initio EDP calculated for the airglow theory presented above shows that the ab initio EDP is consistently low (Figure 13). Eventually we want a method of adjusting the input parameters of our EDP calculation which can bring the calculated EDP into line with the measured EDP without destroying the fit of the calculated airglow emission to the observed airglow. However, for this case we simply tried changing the neutral atmosphere to fit the model EDP to the measurements at the F2 peak (Figure 13).
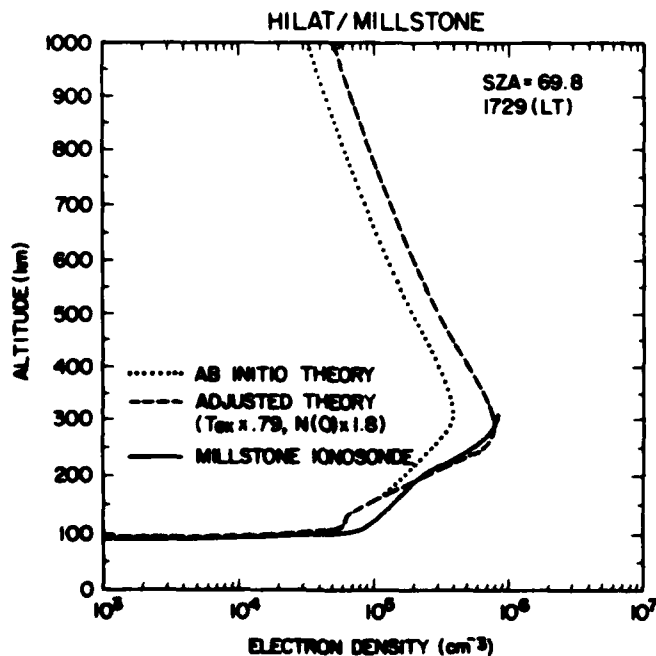
Figure 13. Case Three: A Comparison of the Calculated and Observed Electron Density Profile

Case Four: White Sands Missile Range, 9 January 1978. In this case we modeled 1356 A emission data from nadir-viewing measurements made by a FUV spectrometer flown on a NASA rocket experiment (Anderson et al[4]). Also available was an EDP whose bottomside was based on White Sands ionosonde data while its topside was an extrapolation of that data. Figure 14 shows the volume emission rates, $V_i(z)$, of OI 1356 A and the LBH bands plotted as a function of altitude. This figure illustrates that the major source of these features is the lower ionosphere.
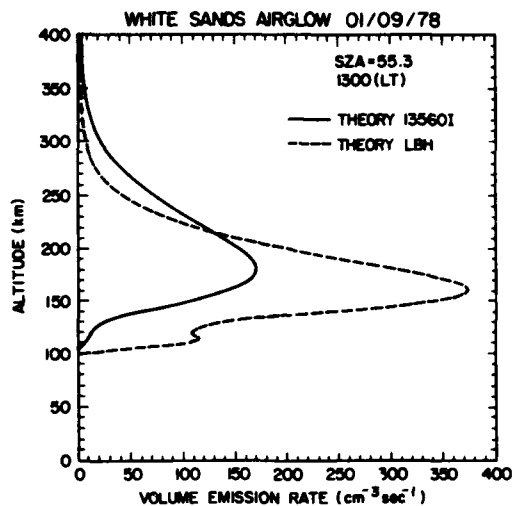
Figure 14. Case Four: White Sands Missile
Range, 9 January 1978. Altitude profiles of
the volume emission rates of OI 1356 A and
the N_2 LBH bands are shown

Figure 15 contains the calculated column emission rate for OI 1356 A and
LBH 1354 A compared to 1356 A emission measurements. We see that theory
basically overestimates the data. Perhaps the more interesting point is again the
illustration of how the bottomside is the source region for the 1356 A feature. A
nadir viewing instrument at 150 km records a dramatically lower emission rate
than an instrument at 250 km, while instruments at 300 km, 400 km or higher will
measure essentially the same rate.

Finally a comparison (Figure 16) of our ab initio EDP calculation with the
measured EDP shows the theory consistently low. We tried adjusting the N_2 and
O_2 densities, as shown in Figure 16, which did improve the fit at low altitudes.
However, the figure also illustrates the unimportance of these two neutral species
at higher altitudes.

30
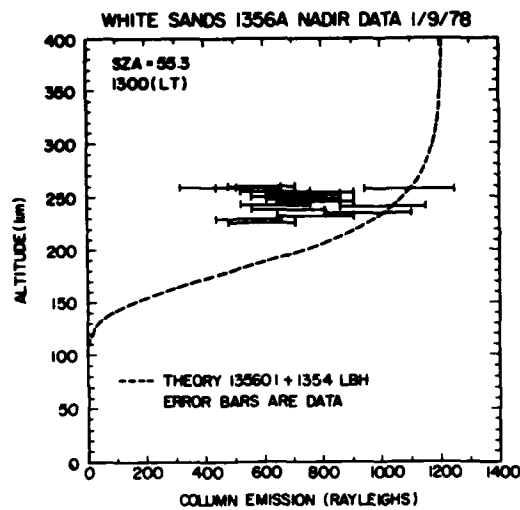
Figure 15. Case Four: A Comparison of the Calculated and Observed Column Emission Rate of OI 1356 A
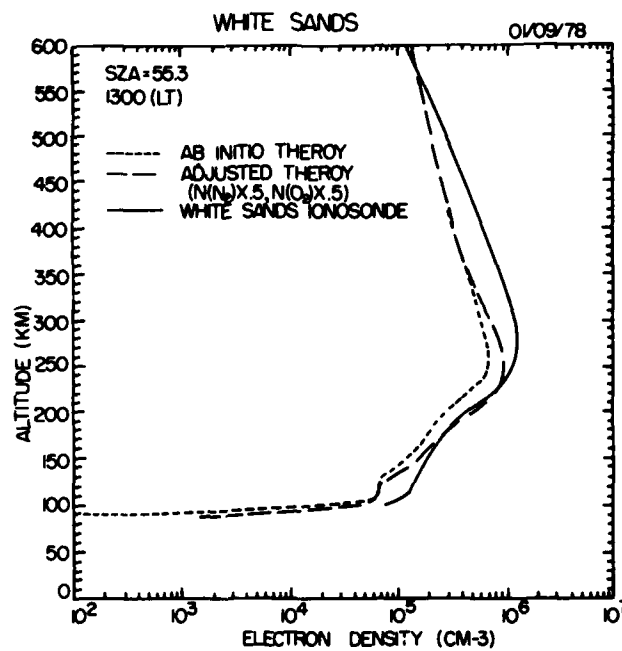
Figure 16. Case Four: A Comparison of the Calculated and Observed Electron Density Profile. The "observed" topside ionosphere is extrapolated from the bottomside sounder data

31

Case Five: S3-4, Rev 2386/Boulder, 10 August 1978. We again had optical emission data from the nadir viewing spectrometer on board S3-4. We also had ground based ionosonde data taken within 5 min of the S3-4 satellite passing overhead.

We found our ab initio modeled EDP was below the ionosonde derived EDP, (see Figure 17). Moreover our calculated 1356 A and 1383 A emissions equaled 73 percent and 48 percent respectively of the measured features. We attempted to improve the calculation by increasing the solar flux. Near 90 km the electron density scaled as the square root of the solar flux, while at higher altitudes (250 km and above) the dependence was more nearly linear. This scaled solar flux also increased the calculated 1356 A feature to 1.08 times the measured 1356 A feature, while the calculated 1383 A increased to 71 percent of the measured 1383 A emission.
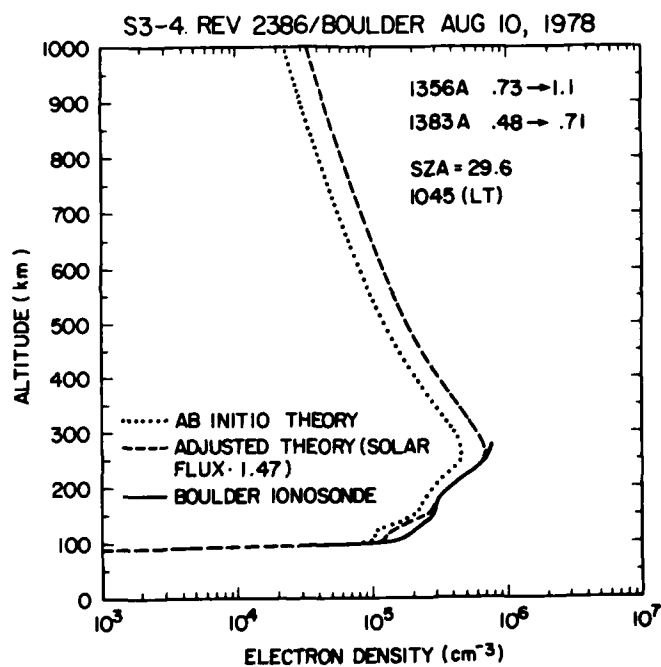
Figure 17. Case Five: S3-4, Rev 2386, and Boulder Ionosonde, 10 August 1978. The EDP derived from bottomside sounder data is compared to the ab initio model

32

3.4 Discussion

We can draw several conclusions from our case studies of comparisons between theory and experiment.

(1) We can model the essential features of the EDP and certain UV emissions.

(2) The models are sensitive enough in general to their input parameters that using "typical" estimates of these parameters can produce poor absolute agreement between theory and experiment.

(3) By reasonable adjustments of the input parameters we can produce excellent agreement between theory and the data for either EDP or optical emissions. However, obtaining good agreement between theory and experiment for both EDP and optical emissions is more difficult.

(4) Our qualitative understanding of the relationship between certain input parameters—the solar flux and neutral densities—and the model EDP and airglow features has been verified.

In FY85 we will continue with two types of studies. First, a systematic parameter study will be made of our models. From this study, we will quantify the relationship between the input parameters and the EDP and the optical emissions. Our goal is to have the capability to efficiently vary the input parameters to produce desired EDPs and airglow features.

We will also establish from the parameter study the range of parameter values that can produce the same values for a set of airglow emissions. From this information we can determine for a given set of emission measurements how much variability in the model EDP is consistent with those measurements. This in turn will allow us to specify what other information, besides airglow data, will be necessary in order to predict the EDP to some desired accuracy.

Our other study will be a continued analysis of coincident EDP and airglow data. This will test our ability to produce good absolute agreement with both EDP and airglow measurements, as well as develop statistics on the reliability of our modeling.

33

4. NIGHTTIME MIDLATITUDE IONOSPHERE

4.1 Prior Work

During the previous fiscal year (FY 83), we extensively investigated the use of UV and visible airglow emissions for monitoring the nighttime ionosphere (Strickland et al[1]). Tinsley and Bittencourt[20] and Chandra et al[21] discovered that the intensities of several atomic oxygen emission lines could be used to infer ionospheric parameters. We investigated the feasibility of the technique they proposed (the Chapman layer model, described in Section 4. 3) as well as the detectability of the necessary emission lines. We concluded that the technique was viable and that the emission lines could be measured using existing technology. However, many details of the measurement and data analysis processes remain to be defined.

To characterize the ionosphere, the intensities of two atomic oxygen emission features must be measured. One of these must be the red line at 6300 A. The other can be any one of several features. From the ground, the line at 7774 A is most useful, but from space the UV line at 1356 A is best. The line at 1304 A can also be used, but it is optically thick and requires more analysis than the other lines.

The 6300 A line comes from excited oxygen atoms which are produced by dissociative recombination of O_2^+. The sole source of O_2^+ in the quiet nighttime ionosphere is charge exchange between O^+ and O_2. Thus the O_2^+ density is closely related to the O^+ density. The other features mentioned above are produced by radiative and ion-ion recombination of O^+. Since the O^+ density is very nearly equal to the electron density in the F region, these emission features are directly related to the EDP. However, when viewed by a nadir pointing or zenith pointing instrument, they give information on the integrated electron density. To infer an altitude profile, one must use a model. In the simplest case, one may assume a parameterized shape function for the EDP and determine the values of the parameters from the intensities of the 6300 and 1356 A lines. The two parameters used in the Chapman layer model are the maximum electron density ($N_m F_2$) and the height of the maximum ($h_m F_2$). A more sophisticated approach would involve calculating the shape based on first principles. During fiscal 1983, we concentrated on the Chapman layer model.

On the basis of published observations and our own model calculations we established the extreme intensity ranges likely to be encountered at night. On the

20. Tinsley, B. A., and Bittencourt, J. A. (1975) Determination of F-region height and peak electron density at night using airglow emissions from atomic oxygen, J. Geophys. Res. 80:2333.

21. Chandra, S. E., Reed, E. I., Meier, R. R., Opal, C. B., and Hicks, G. T. (1975) Remote sensing of the ionospheric F-layer by use of OI 6300 and OI 1356 A observations, J. Geophys. Res. 80:2327.

basis of our investigations, we concluded that the intensity of the 1356 A line can be measured by existing UV photometers, even at the low end of the range. However, the sporadic appearance of N_2 LBH bands detected by Huffman et al[8] would render the measurement extremely difficult whenever they were present. The cause of these bands at night remains unknown, and their presence has not been detected by all satellite UV experiments. Its impact on the proposed system remains under investigation.

Although the 6300 A line is brighter than the 1356 A line, its measurement is beset by other difficulties due to its location in the visible part of the spectrum. Because the atmosphere is transparent to visible light, light from the moon and stars is reflected from the ground and from clouds. The 6300 A line is itself reflected, and the reflected portion must be subtracted to obtain an accurate measurement of the actual emitted intensity. Our investigations indicated that the required background subtractions could be performed if a tilting filter photometer or its equivalent were used. However, many details of the data analysis process remained to be worked out.

Our examination of the Chapman layer model led us to conclude that the technique is not only viable but can be considerably more accurate than existing ab initio models. Comparisons between EDPs deduced by this technique and ionosonde measurements generally give good agreement. However, coincident measurements of the airglow and electron densities at night are rare, and none of the optical experiments were designed with this technique in mind. Although it is clear that the basic technique is sound, it is also clear that care must be given to instrument calibration, instrument sensitivity, and background removal if accurate results are to be obtained.

During FY84 we continued our investigations of the concerns described above with emphasis on the detectability problem. We also began studying a dynamical hybrid model of the nighttime ionosphere which may provide more accurate EDPs than the Chapman layer model. These two competing approaches are described in Sections 4.2 and 4.3. Our latest work on the detectability is described in Section 4.4, and our present assessment of the status of the nighttime problem is presented in Section 4.5.

4.2 Approach 1: Dynamical Hybrid Model

One approach to modeling the nighttime midlatitude EDP is to solve an initial value problem. Starting at sunset with an initial value for the EDP, the E region quickly decays away while the F region can be followed through the night by tracking the solution of the O^+ time dependent continuity equation. Further, in contrast to

35

the daytime situation, nighttime emission features such as 1356 A and 6300 A are directly related to the EDP.

We are in the early stages of developing codes which will solve this initial value problem for the nighttime EDP and derive the related nighttime emissions. To date, no comparisons with nighttime EDP or optical emission measurements have been made.

4.3 Approach 2: Chapman Layer Model

The Chapman layer model assumes that the EDP is always well described by a modified Chapman function. This technique makes use of the direct relation between certain atomic oxygen emission features and the oxygen ion as described in Section 4.1. Radiative and ion-ion recombination of O^+ ions ($O^+ + e \rightarrow O^*$ and $O^+ + O^- \rightarrow O + O^*$, respectively) produces several emission features of which the most useful are the lines at 1356 A and 1304 A. Dissociative recombination of O_2^+ ($O_2^+ + e \rightarrow O + O^*$) results in a single useful feature, the line at 6300 A. In the following discussion we will assume that the two features to be used are OI 1356 A and OI 6300 A.

In the Chapman layer model, the intensities of the two features are related to the EDP maximum, $N_m F_2$, and the height of the maximum, $h_m F_2$, by the equations

$$4\pi I_{1356} = g_1(N_m F_2, h_m F_2) \tag{7}$$

and

$$\frac{\sqrt{4\pi I_{1356}}}{4\pi I_{6300}} = g_2(N_m F_2, h_m F_2) \ . \tag{8}$$

$4\pi I$ is the column emission rate of the feature indicated by the subscript, and g_1 and g_2 are functions whose form depends on the assumed shape of the EDP as well as on chemistry and neutral densities. The dependences of these two functions on $N_m F_2$ and $h_m F_2$ are illustrated in Figures 18 and 19. Note that g_1 depends only on $h_m F_2$, and g_2 depends weakly on $N_m F_2$. To a first approximation, Eq. (1) determines $N_m F_2$, while Eq. (8) determines $h_m F_2$. Better approximations can be obtained by iteration.
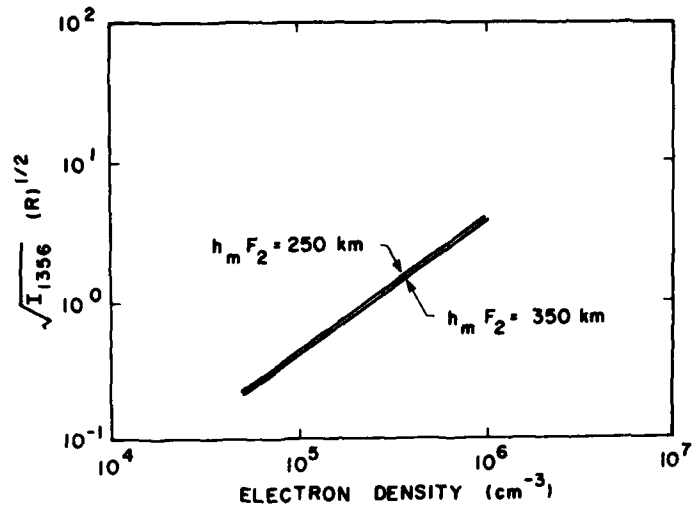
Figure 18. The Dependence of the OI 1356 A Intensity
on the Peak Electron Density, N_mF_2. The ordinate
is the square root of the intensity. It is a linear
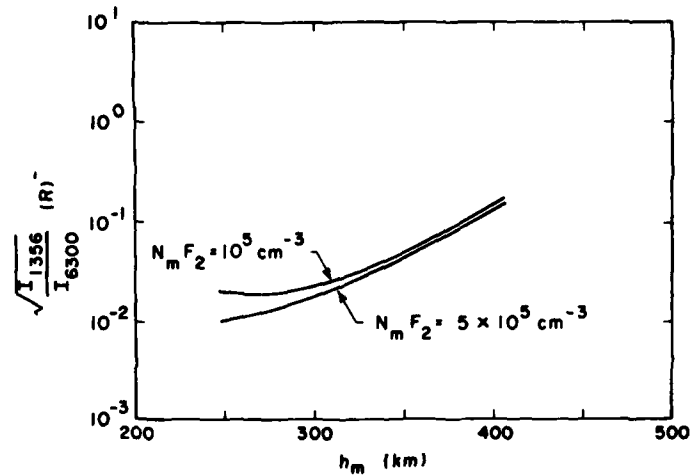function of N_mF_2 and has only a weak dependence on
h_mF_2

Figure 19. The Dependence of the OI 6300 A Intensity
on the Height of the Electron Density Peak, h_mF_2.
The ordinate is the ratio of the square root of the
OI 1356 A intensity to the OI 6300 A intensity. It is
a non-linear function of h_mF_2 and has only a weak
dependence on N_mF_2

37

The two parameters N_mF_2 and h_mF_2, along with a good model neutral atmosphere, uniquely specify a Chapman function approximation to the EDP. We have found that this approximation is quite good even under dynamic transport events such as the post-midnight collapse. Even though the EDP is somewhat distorted in these events, the Chapman function determined by the intensities of OI 1356 A and OI 6300 A provides a good approximation to the actual EDP (that is, it is in error by no more than 30 percent and usually much less). Unless detailed information on neutral winds (which are quite variable) is available, ab-initio calculations can be in error by as much as an order of magnitude.

4.4 Detectability of Weak Ionospheric Emissions

During fiscal 1984 we have investigated the problems associated with measuring the weak airglow emissions at night. Our goal has been to determine the requirements that an instrument must meet in order to make these measurements accurately. We have focused on the particular requirements imposed by the DMSP noon-midnight orbit. At night this orbit is really located at a local time of approximately 2200. To determine the likely ionospheric characteristics at that local time, we have begun to study the f_oF_2 maps produced from topside sounder data by the Japanese Radio Research Laboratories.[22, 23, 24, 25] From these maps, we have determined the ranges of peak electron density (N_mF_2) to be expected at various latitudes. The minimum, maximum, and mean of N_mF_2 for various latitudes are listed in Table 2. These are somewhat higher than we reported in our earlier report. The earlier estimates were based on limited data sets, were quite conservative, and were for various local times. The lowest nighttime densities always come after midnight and usually just before dawn. Since similar maps of h_mF_2 have not been produced, we must rely on ground based data such as the incoherent scatter facility at Millstone Hill. For a local time of 2200, we expect h_mF_2 to fall between 250 km and 350 km at midlatitudes.

The main obstacle to measuring OI 1356 A is its inherent weakness. Table 2 shows the range of intensities expected for OI 1356 A and 1304 A based on the electron densities described above. The minimum expected OI 1356 A intensity is 0.18 R in the midlatitude trough near 60° latitude. To be safe, we should anticipate intensities as low as 0.1 R. Most of the time there is little background radiation near 1356 A. However, the electron drizzle (Torr et al[26]) that is often present at midlatitudes can occasionally stimulate enough 1356 A emission to cause problems at the low end of the range. A more serious problem is the N_2 LBH band emission that has been observed on several occasions (for example, Huffman et al[8]), and whose origin is still unknown (Meier and Conway[27]). It is not seen all the time and seems

---

(Due to the large number of references cited above, they will not be listed here. See References, page 57.)

to be most prevalent for low altitude spacecraft. If it is associated with a spacecraft-atmosphere interaction, it should not be a problem for instruments on DMSP. If it is a genuine atmospheric phenomenon, then it poses a serious problem for those times when it is present. One solution is to measure the atomic oxygen ionization continuum near 911 A which is not affected by LBH emission. Another is to subtract the LBH emission by using a synthetic spectrum normalized to the observed emission from a nearby band. The first solution requires an additional photometer operating in a difficult part of the spectrum. The second requires confidence in our ability to produce a synthetic spectrum for a phenomenon that we do not understand. We plan to continue to investigate this problem.

Although the sources of background for the OI 6300 A line are better understood, they are also more severe. Starlight and the zodiacal light reflected from the "surface" (that is, land, oceans, or clouds) produce a low level background whose intensity depends mainly on the surface albedo. Reflected moonlight produces a background whose intensity ranges from zero when the moon is below the horizon to as much as 500 R A^{-1} at full moon over a high albedo surface (for example, snow). Since all of these sources are broadband, their contribution to the background can be reduced by using an instrument with a narrow bandwidth. Another source of background is the (9-3) band of OH which originates in the middle atmosphere. Of particular concern are the three rotational lines at 6287 A, 6298 A, and 6307 A (Hernandez[28] and Burnside et al[29]). In addition, one must be careful about the choice of wavelength at which the background is to be monitored since there are several nearby absorption lines of molecular oxygen.

Because of its brightness, reflected moonlight requires special consideration. The intensity observed by a nadir viewing instrument depends on the phase of the moon, the declination of the moon, the lunar zenith angle, the latitude and local time of the satellite, and the surface albedo. For approximately half of each lunar month (depending on latitude and season) the moon is below the horizon and contributes nothing to the background. The maximum intensity occurs at or near full moon when the satellite is over snow or clouds (maximum albedo about 0.95 for either). Because the DMSP satellite is at 2200 LT, it is never exposed to the maximum reflected moonlight intensity. At midlatitudes the maximum intensity is less than 400 R A^{-1} and falls to about 200 R A^{-1} at the midlatitude trough. Table 3 lists the maximum moonlight intensity, the intensity at half moon (first quarter only), and the minimum, maximum, and mean OI 6300 A intensities for several latitudes.

28. Hernandez, G. (1974) Contamination of the OI ($^3P_2$-$^1D_2$) emission line with the (9-3) band of OH X$^2\Pi$ in high-resolution measurements of the night sky, J. Geophys. Res. 79:1119.

29. Burnside, R.G., Meriweather, J.W., Jr., and Torr, M.R. (1977) Contamination of ground-based measurements of OI (6300 A) and NI(5200 A) airglow by OH emissions, Planet. Space Sci. 25:985.

Table 2. Expected Nighttime Intensities of OI 1356 A and 1304 A at a Local Time of 2200. The OI 1304 A intensities were calculated using $h_m F_2$ = 350 km. The high and low latitude data are included for information only. We expect optical emissions to be useful only in the midlatitude region (approximately 20° to 60°)

Latitude (degrees)	$N_m F_2$ (10^5 cm^{-3})			OI 1356 A (R)			OI 1304 A (R)		
	Minimum	Maximum	Mean	Minimum	Maximum	Mean	Minimum	Maximum	Mean
80	2.0	4.0	3.2	0.72	2.9	1.8	1.2	4.9	3.1
70	1.5	3.5	2.7	0.40	2.2	1.3	0.68	3.7	2.2
60	1.0	3.2	2.4	0.18	1.8	1.0	0.31	3.1	1.7
50	1.2	5.6	2.4	0.26	5.7	1.0	0.41	9.7	1.7
40	1.1	8.5	3.0	0.22	13	1.6	0.37	2.2	2.7
30	2.0	10	5.0	0.72	18	4.5	1.2	31	7.7
20	5.2	18	9.2	4.9	59	15	8.3	100	26
10	2.9	15	9.2	1.5	41	15	2.6	70	26
0	6.4	16	12	7.4	47	26	13	80	45

40

The detectability of any airglow feature cannot be properly assessed without also discussing instrument capabilities and requirements. Since this involves integrating the requirements imposed by the special problems of all of the regions to be monitored, we defer that discussion to Section 6.

Table 3. Expected Nighttime Intensities of Reflected Moonlight and OI 6300 A at a Local Time of 2200. The OI 6300 A intensities were calculated using the electron densities of Table 2 and h_mF_2 = 350 km. The moonlight values are for a surface (or cloud) albedo of 0.95. The high and low latitude data are included for illustrative purposes only

Latitude (degrees)	Maximum Reflected Moonlight ($R\,A^{-1}$)	Moonlight at 1st Quarter (Half Moon) ($R\,A^{-1}$)	OI 6300 A (R)		
			Minimum	Maximum	Mean
80	153	24	17	36	28
70	190	27	13	31	24
60	236	28	9	29	21
50	289	29	10	50	21
40	333	26	10	78	27
30	364	24	17	93	45
20	395	23	47	168	85
10	414	22	25	143	85
0	420	22	58	154	107

4.5 Discussion and Conclusions

One issue that affects both of the approaches that we have described (dynamic hybrid and Chapman layer) is the topside ionosphere. Because the observed column intensity is mostly due to emission near and below the maximum electron density, optical emissions provide little information about the topside ionosphere. In particular, they give no information on H^+ which can be the dominant ion at altitudes as low as 600 km at night. The best way to gain information on the topside ionosphere is to measure the electron density (and ion composition, if possible) at the satellite. Then the topside can be specified by interpolation between this point and the peak region. We expect to explore this issue further during fiscal 1985.

Another issue that we plan to study during 1985 is an error analysis of the entire process of inferring the EDP from optical and in situ measurements. This involves quantifying the effects of statistical uncertainties in the optical intensities and in situ densities, as well as studying the error properties of the models themselves. This

41

analysis will be carried out for both the dynamic hybrid and Chapman layer approaches.

Although there remain a number of important issues that must be resolved, we remain convinced that the nighttime ionosphere can be successfully monitored using existing optical technology.

5. THE DIFFUSE AURORAL E LAYER

This section will be brief because the subject was discussed in some detail in last year's AFSD report (Strickland et al[1]) and because this year's emphasis has been on other regions of the global ionosphere. One notable auroral investigation this year, however, has addressed the important subject of how much of the initial auroral electron energy is converted to radiation, dissociation, ionization, and to energy carried by metastable atoms and molecules. We discovered that the fractional energy deposition into these various loss channels is sensitive to the hardness of the electron spectrum. This work was reported at the fall AGU meeting and will be documented in a report being prepared by us for AFGL under a subcontract from the Applied Physics Laboratory of Johns Hopkins University.

Our past work and last year's report focussed on the diffuse auroral E layer on the nightside part of the auroral oval. We are just beginning to investigate the daytime auroral problem, which is important since daytime auroras are common occurrences and since the dayside of the oval is an important source of F region plasma for the polar cap and at times for the nightside of the oval (see for example, Weber et al[30]). The emphasis in this section will be on diffuse aurora in the daytime.

5.1 Prior Work

A good overview of our prior work is given in Section 5 of last year's AFSD report. Our approach has been to do first-principles modeling using state-of-the-art electron transport techniques and to determine the sensitivity of the EDP and key optical emissions to changing auroral conditions. Two recent papers documenting this work for emissions in the FUV and MUV are Strickland et al[31] and Daniell and Strickland.[32] Strickland et al[33] also reported on key auroral EUV emissions in which they gave predicted brightnesses under various conditions and began analysing UC Berkeley data obtained on satellite STP 78-1 (Bowyer et al[34] and Paresce et al[35]). This was presented at the fall AGU meeting and has not yet been prepared for publication. It has been documented in an AFGL quarterly report and may be obtained

(Due to the large number of references cited above, they will not be listed here. See References, page 57.)

from the authors upon request. Our work is to a stage of maturity where we believe we can firmly quantify the key optical emissions from the EUV to the visible region and quantitatively relate them to E layer EDPs. As stated at the end of Section 5 in last year's report (Strickland et al[1]), however, we still need to better quantify the error bars on EDPs deduced from nadir viewing satellite optical data.

5.2 Electron Densities and Optical Intensities: Nighttime

Examples were given in last year's report in the form of a Chatanika radar deduced EDP, FUV data from two rocket experiments, and numerous predicted intensities. We refer the reader to this report for optical information. It is worth showing again an example of EDP's, (see Figure 20). The figure is taken from Weber et al[30] and shows five Chatanika radar observed EDPs as well as predictions at various horizontal distances north of the radar site itself. The predictions were made with our auroral electron transport/chemistry model and used DMSP observed electron spectra as inputs. (See Hardy et al[36] for a description of the DMSP experiment.) We have three reasons for showing this figure: (1) it provides examples of typical E layer EDPs under diffuse or continuous auroral conditions; (2) we see that good agreement can be achieved between theory and experiment in this region; (3) it demonstrates that serious differences arise once we enter the auroral F region. This problem is discussed in some detail by Weber et al.[30] We just note that the differences are caused by convection, which at times transports plasma 'blobs' into the region.

5.3 Electron Densities and Optical Intensities: Daytime

The continuous aurora is a phenomenon which encircles the magnetic pole and thus is present at all local times. It overlaps the auroral oval in the night sector but lies equatorward of it in the daytime. Whalen[13] provides a good review of the subject giving morphological information that includes latitude and local time variations in energy content and mean energy of the precipitating particles. We will not present examples of EDPs or optical intensities here but note that the daytime continuous E layer can be expected to be similar to that shown in Figure 20. The daytime E layer is, however, on the average, somewhat weaker than that at night.

A complication not present on the nightside arises from solar EUV energy deposition in the F region. This enhances the EDP in the F region but also increases the intensities of certain features, such as OI 1356 A. Increases worth noting can also take place in N_2 LBH bands if the solar zenith angle falls below approximately 80 degrees.

---

36. Hardy, D.A., Gussenhoven, M.S., and Huber, A. (1979) The Precipitating Electron Detectors (SSJ/3) for the Block 5D/Flights 2-5 DMSP Satellites: Calibration and Data Presentation, AFGL-TR-79-0210, AD A083136.
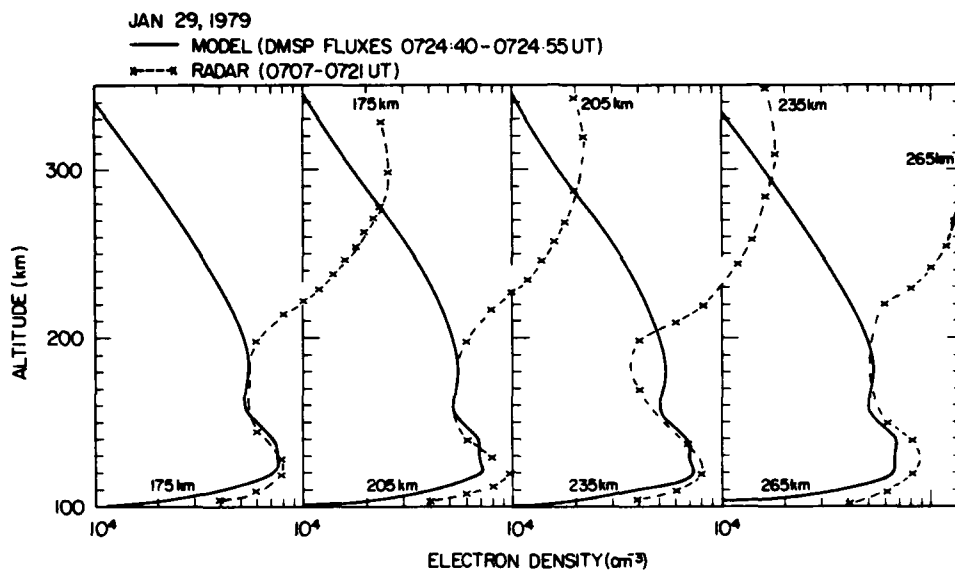
Figure 20. Calculated and Observed Auroral Electron Density Profiles. The data (dashed curves) are from the Chatanika radar facility. The model calculations (solid curves) are based on electron fluxes measured by DMSP. Each pair of curves is labeled by the distance north of Chatanika (from Weber et al[30])

The cusp region, although separate from the continuous aurora, is worth noting since it is an important source of F region plasma and has received considerable attention in recent years (see for example, Shepherd[37] and Whitteker et al[38]). Precipitation into this region is very soft and more or less continuous due to direct access to magnetosheath plasma. We have performed some limited investigation of the behavior of this region through calculations starting with incident electron spectra with mean energies around 100 eV. They will not be discussed here, however, since emphasis is on the E region (which is insignificant in the cusp region).

5.4 Modeling of the Daytime Auroral E Layer

This subsection will discuss a task on which we plan to work this next year. It is our intent to extend our predictive capabilities into the daytime auroral ionosphere. To do so requires adding the capability to do photoelectron transport since solar

37. Shepherd, G.G. (1979) Dayside cleft aurora and its ionospheric effects, Rev. Geophys. Space Phys. 17:2017.

38. Whitteker, J.H., Shepherd, G.G., Anger, C.D., Burrows, J.R., Wallis, D.D., Klumpar, D.M., and Walker, J.D. (1978) The winter polar ionosphere, J. Geophys. Res. 83:1503.

44

radiation will be present at large solar zenith angles. As in the case of the night-time auroral ionosphere, two issues must be addressed. The first addresses the question of how well the EDP and optical intensities can be calculated given the key inputs (neutral densities, temperatures, and sources of ionization and excitation). The second addresses the question of how well the EDP can be deduced from optical data. The issues, although related, are distinct since for the latter, direct informa-tion is not given on the key inputs and uncertainties in the optical data loom as a potentially important source of error in the deduced EDP. Here, we will primarily discuss the first issue with the intent of working on both issues this next year.

We start, however, with some thoughts on how the added solar source will affect the determination of the auroral E layer from optical data. In terms of emission, the added solar source will primarily enhance intensities of the O features such as OI 1356 and OI 1304 A. N_2 LBH bands will have negligible enhance-ment since the photoelectrons cannot penetrate far enough into the E region to cause any significant excitation of N_2. This is in contrast to normal daytime conditions where the solar zenith angle is smaller leading to photoelectron production down to lower altitudes. Since we wish to use both N_2 and O emissions to deduce the daytime auroral E layer EDP, it will be necessary to model the photoelectron production and transport and the associated excitation of O states such as ^5S. With accurate estimates of this excitation, the emission contribution from photoelectron excitation may be subtracted from the total intensity reducing the problem to the nighttime case. *We will be determining this next year how accurately one can expect to calcu-late the photoelectron component of the O emissions.*

Proper modeling of the problem requires a calculation of the transport of both auroral electrons and photoelectrons. The transport equation for a single consti-tuent is

$$\mu \frac{d\phi}{dz} (z, E, \mu) = -K(z, E) \, \phi (z, E, \mu)$$

$$+ K(z, E) \int R(\mu', \mu, E', E) \, \phi (z, E', \mu') dE' \, d\mu' \qquad (9)$$

$$+ S(z, E, \mu)$$

with the following definitions:

z, E, and μ	Altitude, energy (eV), and direction cosine.
$K(z, E)$	Inverse mean free path (density times total cross section).

$R(\mu', \mu, E', E)$ Redistribution function for the scattering of an electron from E', μ', to E, μ.

$\phi(z, E, \mu)$ Electron flux in units of e/cm^2-sec-eV-sr.

$S(z, E, \mu)$ Internal source function (in this case, describing photoelectron production) in units of e/cm^3-sec-eV-sr.

We use a multiconstituent form of the transport equation but show the single constituent version for ease of illustration.

The auroral transport code is designed to easily accommodate additional source terms brought in through S. We also have the code needed to specify S for either large or small solar zenith angles. The transport code will be run with and without S to obtain pairs of the solution ϕ. These will then be used to obtain volume emission rates using

$$P_{jk}(z) = n_j(z) \int \sigma_{jk}(E') \, \Phi(z, E') \, dE' \qquad \text{photons}/cm^2\text{-sec} . \qquad (10)$$

where Φ is the spherical flux (ϕ integrated over 4π), n_j is the density of the species colliding with the electrons and σ_{jk} is the cross section for this species leading to the kth excited state, which produces the emission. Pairs of intensities will be calculated and compared to study the effect of adding the solar source. This will be done as a function of the following parameters:

(1) incident auroral electron spectrum,
(2) neutral density profiles and temperature, and
(3) solar spectrum and solar zenith angle

Ion densities and the E region EDP will also be calculated for variations in the above parameters. They will not be affected, however, by item 3 since the solar source primarily affects the F region EDP. This part of the study is then identical to its counterpart for the nighttime continuous aurora which has produced a large body of results.

6. REQUIRED INSTRUMENT CHARACTERISTICS

6.1 Optical Emissions

Table 4 lists nominal column emission rates for some of the candidate optical features for the three global regions of interest. The nighttime emission rates are much lower than either the daytime or auroral rates. This has important implications for system design. On the other hand, the table does not show that the daytime

46

and auroral spectra contain many more features than the nighttime spectrum, and this also has implications for system design. In general, sensitivity is more important than spectral resolution for measurement of nighttime features, while the opposite is true for measurement of daytime and auroral features. These considerations indicate that it is unlikely that a single system can be designed to meet the requirements of all three ionospheric regions.

Table 4. Nominal Ranges of Column Emission Rates in Rayleighs as Would be Observed From DMSP. Missing entries indicate that the feature is not useful in that region

Feature	Day	Auroral E-Layer	Midlatitude Night
OI 911			0.09 - 30
OI 1304	1000 - 20,000	1000 - 10,000	0.03 - 100
OI 1356	100 - 3000		0.1 - 60
OI 6300			9 - 170
LBH 1273	5 - 50	10 - 50	
LBH 1325	10 - 100	20 - 100	
LBH 1383	20 - 200	30 - 150	
LBH 1672	10 - 100	20 - 100	
LBH 1752	10 - 100	20 - 100	

Although the UV emission features at night are quite weak, existing UV photometer technology can measure them with sufficient accuracy and with reasonably short integration times. The OI 6300 A feature presents a completely different set of problems. These are illustrated by a portion of the nightglow spectrum taken from the ground by Broadfoot and Kendall[39] (Figure 21). It shows two separate sources of background: a continuum from astronomical sources (moonlight, starlight, and the zodiacal light) and discrete lines of the OH vibration-rotation bands. There is an additional problem which is unique to observations from satelittes: the albedo of the earth. Since the atmosphere is transparent to visible light, some fraction of the OI 6300 A light emitted in the downward direction will be reflected upward by the surface or clouds. The intensity of this reflected light must be subtracted from the measured intensity so that the true column emission rate can be determined.

39. Broadfoot, A. L., and Kendall, K. R. (1968) The airglow spectrum, 3100-10,000 A, J. Geophys. Res. 73:426.

Fortunately, the astronomical background provides a means of determining the surface albedo since it is, in principle, known a priori. We propose the use of a tilting filter photometer, or equivalent system, for monitoring the signal, the background, and the albedo. The data analysis methods required by this instrument are described below.
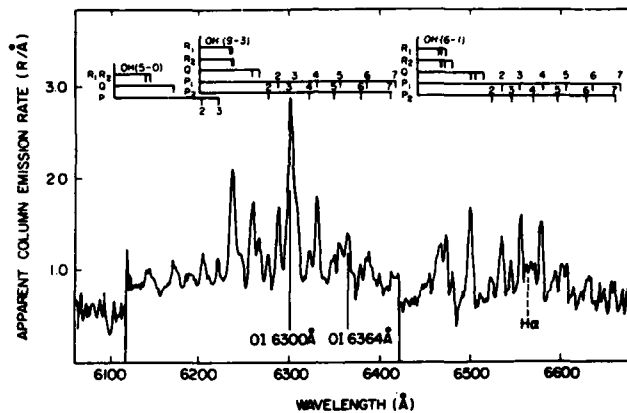
Figure 21. An Example of the Airglow Spectrum in the Vicinity of 6300 A. The spectrum was obtained from the ground (Broadfoot and Kendall[39]), and illustrates two sources of background: the astronomical continuum and the discrete lines of the OH ground state vibration-rotation bands

Some examples of synthetic spectra for auroral and daytime conditions are shown in Figures 22 and 23. (Optically thick features like OI 1304 A have been left out.) The richness of the spectra is readily apparent. The spectral resolution of existing UV photometers is inadequate to separate all of these features. Fortunately, the intensities are large enough that existing UV spectrometer technology is quite satisfactory for both spectral resolution and sensitivity. Note that the intensities of many of the features vary with environmental conditions (for example, electron energy for the auroral ionosphere and solar activity for the daytime ionosphere). This is the basis for the proposed method of using UV emissions to monitor the EDP.

Figure 22. Synthetic Spectra for Nighttime Auroral
Conditions. The dependence of the emission rates
on the characteristics of the ionization source
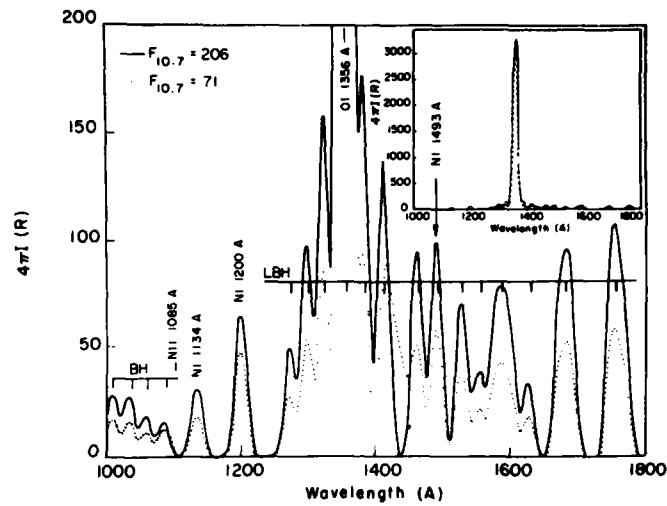(precipitating electrons) is the basis for the remote
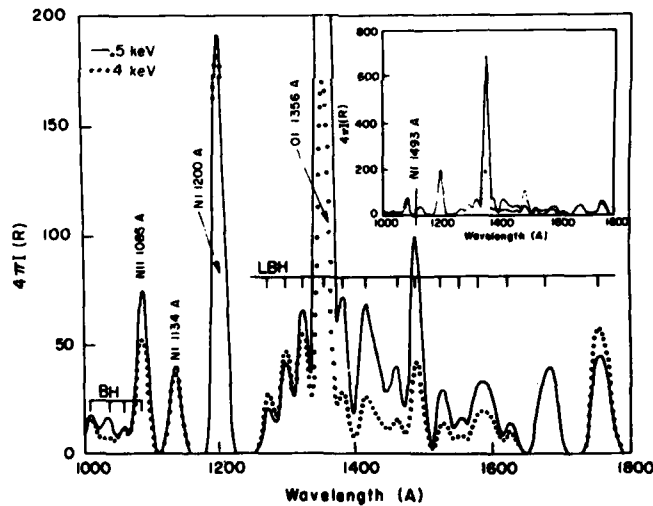sensing technique

Figure 23. Synthetic Spectra for Daytime Mid-
latitude Conditions. The dependence of the
emission rates on the characteristics of the
ionization source (solar EUV photons) is the
basis for the remote sensing technique

49

6.2 The Monitoring System

We anticipate that the optical monitoring system will consist of two subsystems. The first subsystem will be a UV spectrometer intended for monitoring the dayglow and aurora, although it may also have some role to play at night. The second subsystem will consist of two photometers, one for ultraviolet and one for visible wavelengths. The spectrometer may prove useful for monitoring the nighttime UV background and even for making primary measurements at low latitudes.

A high resolution instrument is required for measuring the important UV spectral features in the dayglow and aurora. These features include OI 1356 A and one or more of the N_2 LBH bands at 1383 A, 1672 A, and 1768 A. A UV photometer with a resolution of 100 A (about the best that can be done at ultraviolet wavelengths) is not able to isolate these features from nearby unwanted features. Spectrometers with resolutions of a few angstroms have been flown on satellites for a number of years. The UV imaging spectrometer designed by AFGL for use on the Polar Bear satellite will be able to monitor the OI 1356 A line and one or more of the LBH bands simultaneously. This is a highly desirable feature.

At night, where sensitivity is more important than spectral resolution, a UV photometer is essential. It can be designed to monitor OI 1356 A exclusively, or to monitor both OI 1356 A and OI 1304 A together. The latter option reduces the sensitivity requirements for the photometer, but it introduces the need to model the optically thick OI 1304 A line. Because of the poorly understood sporadic N_2 LBH background discussed in Section 4.4, it will be necessary to monitor other wavelengths. This can be done by using a filter wheel so that the same photometer can monitor several wavelength bands (but not simultaneously), or by using the UV spectrometer. These considerations and conclusions are discussed more quantitatively below.

The visible photometer for the nighttime subsystem must have both sensitivity and resolution. Fortunately, modern technology has provided us with the necessary tools for accomplishing this. Interference filters at visible wavelengths can be made with bandwidths as small as 2 A (full width at half maximum). Since the central wavelength of these filters varies with the angle of incidence of the incident light, they can be used for limited scanning in wavelength. When coupled with state-of-the-art photometers, the sensitivity is adequate for all but the weakest signals. Thus the tilting filter photometer can be used to monitor both the signal and the background. The data analysis required to pull the signal from its background is described below.

50

6.3 Considerations Applicable to UV Measurements

In order to quantify the sensitivity requirements for the UV instruments we introduce R, the instrument sensitivity or response function. The response function for any optical system is

$$R = \frac{10^6}{4\pi} \, A \, \Omega \, Q \, T \tag{11}$$

where A is the aperture area, Ω is the solid angle field of view, Q is the quantum efficiency, and T is the transmission function. If A is given in cm^2 and Ω in sr, then Eq. (11) gives R in counts/Rayleigh-sec. (This is the inverse of the radiance scaling factor of Huffman et al.[8]) The aperture, field of view, and so on, are subject to engineering constraints not considered in this report, so we will not attempt to specify their values. In the following discussion we will specify only the minimum value of R that is required to make the measurements.

Let us first consider the UV spectrometer. Huffman et al[8] described the UV spectrometer flown on the satellite S3-4. At 1356 A it had a sensitivity of 55 cts $R^{-1}sec^{-1}$ at a wavelength resolution of 25 A. This provides a guide to feasible sensitivity requirements for the spectrometer. For the S3-4 instrument, the dark count rate was about 6 cts sec^{-1} outside the polar regions and up to 7 times higher at polar latitudes. Table 5 shows the sensitivity required to measure the expected minimum OI 1356 A intensity with a statistical uncertainty of 20 percent or less. The required sensitivity is shown for a variety of integration times for each of the three regions of interest. While it is clear that a spectrometer similar to the S3-4 instrument could handle the expected dayglow and auroral intensities, it is clear that the integration times required at night would be too long. (The DMSP satellite covers a distance of about 450 km in 60 sec.)

Now let us consider the capabilities of a UV photometer. The S3-4 satellite also carried such an instrument (Huffman et al[8]), and it had a sensitivity of about 1200 cts R^{-1} sec^{-1} and a dark count rate of 4 cts sec^{-1} outside the polar regions. Table 6 shows the required sensitivity for two cases: a photometer measuring OI 1356 A alone, and a photometer measuring the combined intensity of OI 1356 A and OI 1304 A. Clearly, the integration times are much more reasonable. It will also be desirable to monitor the N_2 LBH background described in Section 4.4. This could be done using the UV photometer with a filter wheel, or by using the spectrometer since the emissions tend to be quite bright when they are present.

51

Table 5. Instrument Response (sensitivity) Required
to Measure the Minimum Expected OI 1356 A Intensities
With an Uncertainty of 20 Percent or Less. The
presence of a dark count of 6 counts/sec has been
assumed

Integration Time (sec)	Required Instrument Response (counts/Rayleigh-sec)	
	Night (0. 1 Rayleigh)	Day and Aurora (100 Rayleighs)
0. 1	2600	2. 6
0. 2	1360	1. 4
0. 5	600	0. 60
1. 0	340	0. 34
2. 0	200	0. 20
5. 0	110	0. 11
10. 0	70	0. 069
20. 0	45	0. 045
60. 0	25	0. 025

Table 6. Instrument Response Required to Detect
OI 1356 A Alone and in Combination With OI 1304 A.
A dark count rate of 4 counts/sec^{-1} was assumed

Integration Time (sec)	Required Instrument Response (counts/Rayleigh-sec)	
	Nighttime	
	1356 Alone	1356 & 1304
0. 05	5100	1700
0. 1	2600	860
0. 2	1300	440
0. 5	570	190
1. 0	310	100
2. 0	180	60
5. 0	93	31
10. 0	59	20

52

6.4 Considerations Applicable to Visible Measurements

In many ways, the measurement of OI 6300 A from space is much more diffi-
cult than any of the UV measurements. The instrument must have a narrow band-
width so that the background is minimized. It must also be sensitive enough to
detect the OI 6300 A signal in the midst of a large background with reasonable
integration times. The best candidate for this job is a tilting filter photometer.
Interference filters with bandwidths of 2 A can be readily obtained, and by tilting
them through small angles, the instrument can scan over a limited wavelength
range. This way the same instrument can monitor the two backgrounds (OH and
astronomical) as well as the signal.

The analysis necessary to determine the required instrument sensitivity is
more complicated than that for the UV instruments because there are two back-
ground sources. Unlike dark count, the background sources in the visible part of
the spectrum are variable in both time and space. This means that the observing
time must be divided among three measurements: the signal and two sources of
background. At times, the necessary integration times will be quite long. In order
to minimize the total integration time, the time that the instrument dwells on a
given feature should be optimized (or nearly so). Since the astronomical background
is a continuum, the intensity detected by the instrument is strongly dependent on the
effective bandwidth of the filter. All these factors must be taken into account in
the analysis.

Before presenting the results of our analysis, we must digress to discuss some
engineering considerations. The bandwidth of an interference filter depends on the
convergence angle of the incident light. For any one filter, the bandwidth is smallest
for parallel light and increases as the field of view increases. The rate of increase
depends on the materials used in constructing the filter, but it is generally quite
small for half angles less than 3°. It increases rapidly for larger angles so that
a half angle of 10° results in a bandwidth as much as four times greater than for
parallel light. It is also true that for filter diameters greater than 50 mm the band-
width increases with filter size. Therefore, for most applications both filter size
and half angle must be kept within reasonable limits.

In most applications, the interference filter is the first optical element in the
system, so the aperture and field of view of the instrument are controlled by the
filter. Since one method for increasing the sensitivity of an optical instrument is
to increase the aperture or field of view or both, the presence of the filter is a
problem. One could increase the aperture by placing a telescope in front of the
filter, but this inevitably means that the half angle of light incident on the filter is
increased. The practicality of this or similar strategies is determined by the
balance between the increased intensity of the continuum background versus the
increased light gathering power of system.

53

The instrument sensitivity required to achieve a specified statistical uncertainty in the presence of a specified background may be determined from the formula:

$$Rt = f(J_{OI}, J_{OH}, J_{astr}, u_{OI}) \tag{12}$$

where t is the total integration time, J_{OI}, J_{OH}, and J_{astr} are the apparent column emission rates of OI 6300 A, OH (9-3) 6287 A, and the astronomical continuum respectively, and u_{OI} is the desired statistical uncertainty in the measurement of J_{OI}. The form of the function f depends on the way the total integration time is divided among the three features. We have derived the form of f appropriate for the optimum division of the total integration time.

Using Eq. (12), we have calculated the value of Rt necessary to detect the minimum expected OI 6300 A signal with a statistical uncertainty of no more than 20 percent in the presence of a typical OH background (5 R) and full moonlight over snow or clouds for several latitudes (Table 7). We have considered several different bandwidths (full width at half maximum): 2.5 A, 5.0 A, 7.5 A, and 10 A. For each case we optimized the dwell time for each feature so that the total integration time was as short as possible consistent with the desired uncertainty. From the table it is clear that the most severe requirement on sensitivity occurs at 40° latitude. In Table 8 we show the required sensitivity for the same four filter bandwidths and for various integration times for those conditions.

Table 7. Values of Rt Required for the Detection of the Minimum OI 6300 A Intensity in the Presence of the Maximum Moonlight Intensity. The indicated bandwidths are full width at half maximum

Latitude (degrees)	Rt (counts/R)			
	2.5 A	5.0 A	7.5 A	10.0 A
80	216	430	645	910
70	455	905	1359	1919
60	1169	2331	3502	4947
50	1155	2304	3461	4890
40	1328	2649	3979	5623
30	503	1002	1505	2125
20	72	143	214	302
10	265	527	791	1117
0	50	100	149	211

Table 8. Instrument Response Required for Detecting
OI 6300 for Various Filter Bandwidths. Worst case
moonlight conditions at a latitude of 40° were assumed.
The indicated bandwidths are full width at half maximum

Integration Time (sec)	Required Instrument Sensitivity (counts/Rayleigh-sec)			
	2.5 A	5.0 A	7.5 A	10.0 A
1	1328	2639	3979	5625
2	664	1325	1990	2813
5	266	530	796	1125
10	133	265	398	563
20	66	132	199	281
30	44	88	133	188
40	33	66	99	141
50	27	53	80	113
60	22	44	66	94

For reference, we have calculated R for a hypothetical instrument with reasonable design parameters:

A = 19.6 cm^2 (50 mm filter)

Ω = 0.01 sr (half cone angle = 3°)

Q = 8 percent

T = 25 percent

R = 312 cts R^{-1} sec^{-1}

We assumed that no optical elements were placed in front of the filter. It may be that state-of-the-art instruments can perform better than this, but this makes a reasonable benchmark. From Table 8 we see that our hypothetical instrument would require less than 5 sec total integration time. Since the DMSP satellite travels about 35 km in this time, our hypothetical instrument is viable. It does not appear that the additional expense and complexity of adding a telescope to the photometer is justified. However, we will continue to study this option.

In order to determine whether it is really necessary to optimize the integration times, we have also calculated the required instrument response assuming that the instrument dwells on each feature for the same amount of time. This method increases the required total integration time by about 25 percent, a nontrivial amount. Again, the instrument designers will have to determine whether making the on board electronics sophisticated enough to optimize the dwell time is cost effective.

55

6.5 Discussion and Conclusions

So far our analysis indicates that no extraordinary technology is required to detect the optical emissions that are most useful for ionospheric monitoring. In the daytime and auroral regions, the high resolution of a spectrometer is essential. The interesting features are bright enough that instrument sensitivity is not a problem. At night, on the other hand, high resolution is not required, but the higher sensitivity of a photometer is essential. This is true for both UV and visible features. Thus we envision an instrument system consisting of a UV spectrometer for use in the daytime and auroral regions and two photometers, one UV and the other visible, for use at night. The spectrometer should be capable of monitoring two features (for example, OI 1356 and one of the LBH bands) simultaneously. The UV photometer may need to have several filters on a filter wheel for background monitoring. The visible photometer should be a tilting filter photometer with the smallest possible bandwidth. At this time, it does not seem necessary to mount a telescope or other optics in front of the filter. We believe that this system can monitor the necessary features with a statistical uncertainty of no more than 20 percent and much less under most conditions.

References

1. Stri land, D. J., Daniell, R. E., Jr., Decker, D. T., Jasperse, J. R., and Carlson, H. C., Jr. (1984) Determination of Ionospheric Electron Density Profiles From Satellite UV Emission Measurements, AFGL-TR-84-0140, AD A150734.

2. Muldrew, D. B. (1965) F-Layer Ionization troughs deduced from Alouette data, J. Geophys. Res. 70:2635.

3. Fejer, D. G., and Kelley, M. C. (1980) Ionospheric irregularities, Rev. Geophys. Space Phys., 18:401.

4. Anderson, D. E., Jr., Meier, R. R., Feldman, P. D., and Gentieu, E. P. (1980) The UV dayglow 3, OI emissions at 989, 1027, 1152, 1304, and 1356 A Geophys. Res. Lett. 7:1057.

5. Strickland, D. J., and Donahue, T. M. (1970) Excitation and radiation transport of 1304 A resonance radiation. I, The dayglow, Planet Space Sci. 18:661.

6. Strickland, D. J., and Rees, M. H. (1974) The OI 1304 A and 1356 A emission in aurorae, Planet. Space Sci. 22:465.

7. Meier, R. R., and Lee, J. -S. (1982) An analysis of the OI 1304 A dayglow using a Monte Carlo resonant scattering model with partial frequency redistribution, Planet. Space Sci. 30:439.

8. Huffman, R. E., Leblanc, F. J., Larrabee, J. C., and Paulsen, D. E. (1980) Satellite vacuum ultraviolet airglow observations, J. Geophys. Res. 85:2201.

9. Hanson, W. B., and Carlson, H. C. (1977) The ionosphere, from The Upper Atmosphere and Magnetosphere, National Academy of Sciences, Washington, D. C.

10. Anderson, D. E., Jr., Meier, R. R., and Weller, C. S. (1976) Observations of far and extreme ultraviolet OI emissions in the tropical ionosphere, Planet. Space Sci. 24:945.

11. Tulunay, Y. K., and Grebowsky, J. M. (1978) The noon and midnight mid-latitude trough as seen by Ariel 4, J. Atmos. Terr. Phys. 40:845.

12. Evans, J. V. (1967) Midlatitude F-region densities and temperatures at sunspot minimum, Planet. Space Sci. 15:1387.

13. Whalen, J. A. (1981) General characteristics of the auroral ionosphere, in Physics of Space Plasmas, Ed. by T. S. Chang, B. Coppi, and J. R. Jasperse, SPI Conference Proceedings and Reprint Series, 4, Scientific Publishers, Cambridge, Massachusetts.

14. Sharber, J. R. (1981) The continuous (diffuse) aurora and auroral-E ionization, in Physics of Space Plasmas, Ed. by T. S. Chang, B. Coppi, and J. R. Jasperse, SPI Conference Proceedings and Reprint Series, 4, Scientific Publishers, Cambridge, Massachusetts.

15. Jasperse, J. R. (1976) Boltzmann-Fokker-Planck model for the electron distribution function in the earth's ionosphere, Planet. Space Sci. 24:33.

16. Jasperse, J. R. (1977) Electron distribution function and ion concentrations in the earth's lower ionosphere from Boltzmann-Fokker-Planck theory, Planet. Space Sci. 25:743.

17. Jasperse, J. R. (1981) The photoelectron distribution function in the terrestrial ionosphere, in Physics of Space Plasmas, Ed. by T. S. Chang, B. Coppi, and J. R. Jasperse, SPI Conference Proceedings and Reprint Series, 4, Scientific Publishers, Cambridge, Massachusetts.

18. Anderson, D. N. (1973) A theoretical study of the ionospheric F region equatorial anamoly, 1, Theory, Planet. Space Sci. 21:409.

19. Stone, E. J., and Zipf, E. C. (1974) Electron impact excitation on the $^3S^0$ and $^5S^0$ states of atomic oxygen, J. Chem. Phys. 60:4237.

20. Tinsley, B. A., and Bittencourt, J. A. (1975) Determination of F-region height and peak electron density at night using airglow emissions from atomic oxygen, J. Geophys. Res. 80:2333.

21. Chandra, S. E., Reed, E. I., Meier, R. R., Opal, C. B., and Hicks, G. T. (1975) Remote sensing of the ionospheric F-layer by use of OI 6300 A and OI 1356 A observations, J. Geophys. Res. 80:2327.

22. Japanese Radio Research Laboratories (1979) Atlas of Ionospheric Critical Frequency (f_oF_2) Obtained From Ionosphere Sounding Satellite-b Observation, Part 1, August to December 1978, Radio Research Laboratories, Ministry of Posts and Telecommunications, Tokyo.

23. Japanese Radio Research Laboratories (1980) Atlas of Ionospheric Critical Frequency (f_oF_2) Obtained From Ionosphere Sounding Satellite-b Observation, Part 2, October 1978 to March 1979, Radio Research Laboratories, Ministry of Posts and Telecommunications, Tokyo.

24. Japanese Radio Research Laboratories (1981) Atlas of Ionospheric Critical Frequency (f_oF_2) Obtained From Ionosphere Sounding Satellite-b Observation, Part 3, January to June 1979, Radio Research Laboratories, Ministry of Posts and Telecommunications, Tokyo.

25. Japanese Radio Research Laboratories (1983) Atlas of Ionospheric Critical Frequency (f_oF_2) Obtained From Ionosphere Sounding Satellite-b Observation, Part 4, August to December 1979, Radio Research Laboratories, Ministry of Posts and Telecommunications, Tokyo.

26. Torr, D. G., Torr, M. R., Hoffman, R. A., and Walker, J. C. G. (1976) Global characteristics of 0.2 to 25 keV charged particles at F-region altitudes, Geophys. Res. Lett. 3:305.

27. Meier, R. R., and Conway, R. R. (1983) On the N_2 Lyman-Birge-Hopfield band nightglow, J. Geophys. Res. 88:4929.

28. Hernandez, G. (1974) Contamination of the OI ($^3P_2$-$^1\Gamma_2$) emission line with the (9-3) band of OH X $^2\Pi$ in high-resolution measurements of the night sky, J. Geophys. Res. 79:1119.

29. Burnside, R.G., Meriweather, J.W., Jr., and Torr, M.R. (1977) Contamination of ground-based measurements of OI(6300 A) and NI(5200 A) airglow by OH emissions, Planet. Space Sci. 25:985.

30. Weber, E.J., Tsunoda, R.T., Buchau, J., Sheehan, R.E., Strickland, D.J., Whiting, W., and Moore, J.G. (1984) Coordinated measurements of auroral zone plasma enhancements, submitted to J. Geophys. Res.

31. Strickland, D.J., Jasperse, J.R., and Whalen, J.A. (1983a) Dependence of auroral FUV emissions on the incident electron spectrum and neutral atmosphere, J. Geophys. Res. 88:8051.

32. Daniell, R.E., Jr., and Strickland, D.J. (1985) Dependence of auroral middle UV emissions on the incident electron spectrum and neutral atmosphere, submitted to J. Geophys. Res.

33. Strickland, D.J., Daniell, R.E., Jr., Chakrabarti, S., and McCoy, R.C. (1983b) EUV spectral variations in aurora—Comparison of theory with satellite data, abstract, EOS, 64:787.

34. Bowyer, S., Kimble, R., Paresce, F., Lampton, M., and Penegor, G. (1981) Continuous readout EUV airglow spectrometer, Appl. Opt. 20:477.

35. Paresce, F., Chakrabarti, S., Bowyer, S., and Kimble, R. (1983) The extreme ultraviolet spectrum of dayside and nightside aurorae: 800-1400 A, J. Geophys. Res. 88:4905.

36. Hardy, D.A., Gussenhoven, M.S., and Huber, A. (1979) The Precipitating Electron Detectors (SSJ/3) for the Block 5D/Flights 2-5 DMSP Satellites: Calibration and Data Presentation, AFGL-TR-79-0210, AD A083136.

37. Shepherd, G.G. (1979) Dayside cleft aurora and its ionospheric effects, Rev. Geophys. Space Phys. 17:2017.

38. Whitteker, J.H., Shepherd, G.G., Anger, C.D., Burrows, J.R., Wallis, D.D., Klumpar, D.M., and Walker, J.D. (1978) The winter polar ionosphere, J. Geophys. Res. 83:1503.

39. Broadfoot, A.L., and Kendall, K.R. (1968) The airglow spectrum, 3100-10,000 A, J. Geophys. Res. 73:426.

END

FILMED

11-85

DTIC